


# Differential Internalization Rates and Postendocytic Sorting of the Norepinephrine and Dopamine Transporters Are Controlled by Structural Elements in the N Termini\*

Received for publication, November 3, 2015, and in revised form, January 7, 2016. Published, JBC Papers in Press, January 19, 2016, DOI 10.1074/jbc.M115.702050

Anne Vuorenpää<sup>‡§¶</sup>, Trine N. Jørgensen<sup>‡</sup>, Amy H. Newman<sup>||</sup>, Kenneth L. Madsen<sup>‡</sup>, Mika Scheinin<sup>§¶</sup> and  Ulrik Gether<sup>‡¶1</sup>

From the <sup>‡</sup>Molecular Neuropharmacology and Genetics Laboratory, Department of Neuroscience and Pharmacology, Faculty of Health and Medical Sciences, Panum Institute 18.6, University of Copenhagen, DK-2200 Copenhagen, Denmark, the <sup>§</sup>Department of Pharmacology, Drug Development, and Therapeutics, University of Turku, Turku FI-20014, Finland, the <sup>¶</sup>Unit of Clinical Pharmacology, Turku University Hospital, Turku FI-20520, Finland, and the <sup>||</sup>Medicinal Chemistry Section, National Institute on Drug Abuse, Intramural Research Program, National Institutes of Health, Baltimore, Maryland 21224

The norepinephrine transporter (NET) mediates reuptake of synaptically released norepinephrine in central and peripheral noradrenergic neurons. The molecular processes governing availability of NET in the plasma membrane are poorly understood. Here we use the fluorescent cocaine analogue JHC 1-64, as well as several other approaches, to investigate the trafficking itinerary of NET in live noradrenergic neurons. Confocal imaging revealed extensive constitutive internalization of JHC 1-64-labeled NET in the neuronal somata, proximal extensions and presynaptic boutons. Phorbol 12-myristate 13-acetate increased intracellular accumulation of JHC 1-64-labeled NET and caused a parallel reduction in uptake capacity. Internalized NET strongly colocalized with the “long loop” recycling marker Rab11, whereas less overlap was seen with the “short loop” recycling marker Rab4 and the late endosomal marker Rab7. Moreover, mitigating Rab11 function by overexpression of dominant negative Rab11 impaired NET function. Sorting of NET to the Rab11 recycling compartment was further supported by confocal imaging and reversible biotinylation experiments in transfected differentiated CATH.a cells. In contrast to NET, the dopamine transporter displayed markedly less constitutive internalization and limited sorting to the Rab11 recycling compartment in the differentiated CATH.a cells. Exchange of domains between the two homologous transporters revealed that this difference was determined by non-conserved structural elements in the intracellular N terminus. We conclude that NET displays a distinct trafficking itinerary characterized by continuous shuffling between the plasma membrane and the Rab11 recycling compartment and that the

functional integrity of the Rab11 compartment is critical for maintaining proper presynaptic NET function.

Reuptake of synaptically released norepinephrine (NE)<sup>2</sup> is the primary mechanism to control duration and strength of noradrenergic neurotransmission. The reuptake is mediated by the NE transporter (NET), which is present in noradrenergic neurons both in the brain and in the peripheral sympathetic nerve system (1–3). NET belongs to the *SLC6* (solute carrier 6) gene family (also referred to as neurotransmitter-sodium symporters) that also includes transporters for the neurotransmitters dopamine, serotonin, glycine, and  $\gamma$ -aminobutyric acid (GABA) (4–6). NET is targeted by many clinically important antidepressant drugs and by several widely abused drugs, such as cocaine and amphetamine. In addition, impaired NET function has been implicated in cardiovascular diseases and in disorders of mood and cognition (7–10).

It is assumed that the amount of NET present in the presynaptic plasma membrane is tightly controlled to sustain NE homeostasis, but the underlying molecular and cellular mechanisms are poorly understood. Several mechanisms have been suggested to regulate NET distribution, including protein kinase C (PKC), whose activation (*e.g.* by  $G_q$ -coupled muscarinic acetylcholine receptors) can increase NET internalization and reduce NE transport capacity (11–14). Furthermore, amphetamine has been shown to decrease NET surface expression, whereas cocaine was found to enhance NET availability (15–17). An elegant study by Galli and co-workers (16) found evidence that the amphetamine-induced decrease in NET surface levels is Rab11-dependent. The general NET trafficking properties and postendocytic sorting pattern, however, have not been investigated in detail. Of interest, several *SLC6* family transporters, such as the dopamine (DAT), serotonin (SERT), and glycine transporters, have been shown to undergo constitutive internalization (18–22). Their fate upon internalization,

\* This work was supported by the FinPharma Doctoral program (to A.V.), National Institutes of Health Grant P01 DA 12408 (to U.G.), the Danish Council for Independent Research-Medical Sciences (to U.G.), the Lundbeck Foundation Center for Biomembranes in Nanomedicine (to U.G.), and the Intramural Research Program, National Institute on Drug Abuse, National Institutes of Health (to A.H.N.). The authors declare that they have no conflicts of interest with the contents of this article. The content is solely the responsibility of the authors and does not necessarily represent the official views of the National Institutes of Health.

<sup>1</sup> To whom correspondence should be addressed: Molecular Neuropharmacology and Genetics Laboratory, Dept. of Neuroscience and Pharmacology, Faculty of Health and Medical Sciences, Panum Institute 18.6, University of Copenhagen, DK-2200 Copenhagen N, Denmark. Tel.: 45-2384-0089; E-mail: gether@sund.ku.dk.

<sup>2</sup> The abbreviations used are: NE, norepinephrine; NET, NE transporter; DAT, dopamine transporter; SERT, serotonin transporter; EGFP, enhanced GFP; SCG, superior cervical ganglion; CAD, differentiated CATH.a; PMA, phorbol 12-myristate 13-acetate; ROI, region of interest; ANOVA, analysis of variance.

however, has not been defined. Whereas some studies suggest that the transporters are recycled back to the plasma membrane (18, 23), other studies support the notion that DAT and SERT primarily are sorted to Rab7-positive late endosomes and subsequently to lysosomal degradation upon both constitutive and stimulated internalization (22, 24, 25).

Here, we employ several different approaches, including use of the fluorescent cocaine analogue JHC 1-64, to describe NET surface distribution, internalization, and postendocytic sorting in live noradrenergic neurons. We show that NET undergoes extensive constitutive internalization and that internalized NET mainly is sorted to Rab11-positive recycling endosomes. Inhibition of Rab11 function by dominant negative Rab11 (Rab11 S25N) impairs NE uptake capacity in noradrenergic neurons, implying that correct and sufficient postendocytic recycling is critical for NET function. Finally, we find that NET displays a markedly higher degree of constitutive internalization than DAT and that this difference, together with the differential postendocytic sorting of NET compared with DAT, is determined in part by non-conserved structural elements in the intracellular N termini of the two transport proteins. Our results reveal striking differences in the trafficking itineraries of NET compared with DAT and provide thereby a critical framework for further deciphering the role of NET and DAT in controlling neurotransmitter homeostasis and how this might be altered in diseased states.

## Experimental Procedures

**Molecular Biology**—The cDNA encoding human NET was kindly provided by Dr. Marc G. Caron (Duke University, Durham, NC) (26). A synthetic gene encoding the human DAT was a kind gift from Dr. Jonathan A. Javich (Columbia University, New York). The enhanced green fluorescent protein (EGFP)-tagged Rab7 and Rab11 constructs (pEGFP-Rab7 and pEGFP-Rab11) were kind gifts from Dr. Katherine W. Roche (NINDS, National Institutes of Health, Bethesda, MD) (27). The plasmid pEGFP-Rab4 was a kind gift from Dr. José A. Esteban (Universidad Autónoma de Madrid, Madrid, Spain) (28). The NET(1–128)/DAT construct was a kind gift from Dr. Bruno Giros (Douglas Mental Health University Institute, Montreal, Canada) (26). The viral vector plasmids pHsSynXW EGFP-Rab4, Rab7, and Rab11 were generated as described previously (20). A DAT/NET(590–617) chimeric construct was generated by introducing a unique restriction site, BsiI, to the coding sequence of NET by PCR. Subsequently, the C-terminal tail of NET was ligated into DAT using digestion with BsiI and XbaI and cloned into pcDNA3.1. DAT(1–59)/NET and NET/DAT(593–620) chimeras were generated by a two-step PCR procedure. First, the N terminus (residues 1–59) and C terminus (residues 593–620) of DAT were amplified from pcDNA3 DAT with primers that generated overhangs identical to the corresponding sequences of NET. Second, the NET parts of the chimeras (NET(56–617) and NET(1–590)) were amplified from NET pcDNA3 with primers that generated overhangs identical to the N and C termini of DAT. Products from the first PCR rounds were used as templates for generating the respective chimeras that were subsequently cloned into pcDNA3.1. TacNET was likewise generated by a two-step PCR procedure.

First, the FLAG-Tac was amplified from pcDNA3 FLAG-Tac with primers generating an overhang identical to the N-terminal part of NET. Second, NET was amplified from pcDNA3 NET with primers with an overhang identical to the C-terminal part of FLAG-Tac. The products from the first round of PCR were used as templates for generating a TacNET fragment that subsequently was cloned into pcDNA3. All constructs were verified by dideoxynucleotide sequencing (Eurofins Genomics, Ebersberg, Germany).

**Glial Coating**—Astrocytes were isolated from rat cerebral cortex and cultured as described previously (29). Astrocytes were seeded on poly-L-ornithine-coated coverslips, Lab-Tek chambers (Nunc), or 96-well plates, cultured approximately for 5 days (to a density of ~70%) and treated with 1  $\mu$ M 5-fluoro-5-deoxyuridine (Sigma) to inhibit further growth.

**Primary Culture of Superior Cervical Ganglion Neurons**—Postnatally derived rat superior cervical ganglion (SCG) neurons were prepared using a protocol modified from that of Savchenko *et al.* (30). Briefly, ganglia from 0–3-day-old rat pups were dissected and dissociated for 30 min at 37 °C in 3 mg/ml collagenase/0.5 mg/ml trypsin in RPMI medium gently oxygenated with a mixture of 95% O<sub>2</sub> and 5% CO<sub>2</sub>. Digestion was terminated by adding 10% fetal bovine serum (FBS) in RPMI medium. Subsequently, cells were briefly centrifuged and then resuspended in warm RPMI medium supplemented with 3% heat-inactivated FBS and 20 ng/ml nerve growth factor (NGF). Digested tissue was carefully triturated into single cells by using increasingly smaller pipette tips. The neurons were seeded onto coverslips coated with glial cells for immunocytochemistry into similarly coated Lab-Tek chambers for live cell imaging or into similarly coated 96-well plates for uptake experiments. On the next day, cultures were treated with 1  $\mu$ M 5-fluoro-5-deoxyuridine to inhibit glial cell growth. Cultures were grown for 12–16 days in supplemented RPMI medium prior to experiments.

**Lentivirus Production and Transduction**—Lentivirus was produced as described previously (20) according to procedures modified from Naldini *et al.* (31). The SCG neuronal cultures were transduced at days 4–5 *in vitro*, and experiments were performed 8–11 days after infection.

**Cell Cultures and Transfections**—Human embryonic kidney (HEK293) cells (ATCC CRL-1573) were grown in Dulbecco's modified Eagle's medium (DMEM) with HEPES and sodium bicarbonate (DMEM 1965), and differentiated CATH.a (CAD) cells (ATCC CRL-11179), originating from mouse brain, were grown in a 1:1 mixture of DMEM 1965 and Ham's F-12 medium (Invitrogen), both supplemented with 10% FBS and 0.01 mg/ml gentamicin. For transient expression, the cells were transfected using standard Lipofectamine 2000 protocols (Invitrogen) 2 days prior to experiments.

**[<sup>3</sup>H]Dopamine Uptake**—NET uptake experiments were carried out using [<sup>3</sup>H]DA (30–60 Ci/mmol, PerkinElmer Life Sciences) as substrate. NET transports DA and NE with similar affinity ( $K_m = 0.5$ – $1 \mu$ M), and [<sup>3</sup>H]DA is commonly used as NET substrate (26, 32–34). Medium was removed from SCG neurons cultured on glial cell monolayers in 96-well plates, and the cells were equilibrated in uptake buffer (25 mM HEPES, pH 7.4, 130 mM NaCl, 5.4 mM KCl, 1.2 mM CaCl<sub>2</sub>, 1.2 mM MgSO<sub>4</sub>, 1

## Internalization and Recycling of NET

mM L-ascorbic acid, 5 mM D-glucose, and 1  $\mu$ M catechol-O-methyltransferase inhibitor Ro 41-0960 (Sigma) for 20 min at 37 °C. Subsequently, phorbol 12-myristate 13-acetate (PMA) (1  $\mu$ M) or vehicle (0.01% DMSO) was added, and neurons were incubated for 30 min at 37 °C. Uptake was initiated by the addition of 100 nM [<sup>3</sup>H]DA, allowed to continue for 5 min at room temperature, and terminated by rapid aspiration of the medium and two washes with ice-cold uptake buffer. Nonspecific uptake was determined in the presence of 100  $\mu$ M desipramine. Opti-Phase HiSafe3 scintillation fluid (PerkinElmer Life Sciences) was added to the wells, and the samples were counted in a Wallac Tri-Lux  $\beta$ -scintillation counter (PerkinElmer Life Sciences).

Saturation kinetics of DA uptake were determined using increasing concentrations of DA (final concentration 0.05–6.4  $\mu$ M) with a trace amount of [<sup>3</sup>H]DA in CAD cells transfected 48 h before the experiment with equal amounts of constructs encoding NET, DAT, NET-DAT chimeras, or TacNET. Uptake was initiated by adding serial dilutions of dopamine/[<sup>3</sup>H]dopamine and was allowed to continue for 3 min at room temperature. Nonspecific uptake was determined in the presence of 100  $\mu$ M nomifensine. Subsequently, cells were lysed in 1% SDS and transferred to counting plates (PerkinElmer Life Sciences), Opti-Phase HiSafe3 scintillation fluid was added, and the samples were counted in a Wallac Tri-Lux  $\beta$ -scintillation counter. Uptake data were analyzed with GraphPad Prism version 5.0 (GraphPad Software, La Jolla, CA).

**Immunocytochemistry**—SCG neurons grown on glial monolayers on coverslips were incubated with 50 nM JHC 1-64 in imaging buffer (25 mM HEPES, pH 7.4, with 130 mM NaCl, 5.4 mM KCl, 1.2 mM CaCl<sub>2</sub>, 1.2 mM MgSO<sub>4</sub>, 5 mM D-glucose) for 20 min at room temperature. Subsequently, the specimens were fixed with 4% paraformaldehyde in phosphate-buffered saline (PBS), blocked and permeabilized in blocking/permeabilization buffer (5% goat serum, 0.2% saponin, PBS), and immunostained with a monoclonal mouse anti-NET antibody (NET-05, mAb Technologies; 1:1000) or a monoclonal mouse anti-tyrosine hydroxylase antibody (Mab318; Millipore, 1:1000) for 30 min at room temperature. Primary antibodies were labeled with a goat polyclonal anti-mouse Alexa Fluor® 488 secondary antibody (Molecular Probes, Inc., Eugene, OR) for 30 min at room temperature. The specimens were mounted on glass slides with Slow-Fade Antifade (Invitrogen) and visualized by confocal microscopy.

**Confocal Microscopy**—Confocal microscopy was performed using a Zeiss confocal laser-scanning microscope (LSM 510) with an oil immersion  $\times$ 63 lens with a 1.4 numerical aperture (Carl Zeiss, Oberkochen, Germany) as described (20). Rhodamine-conjugated JHC 1-64, synthesized according to methods described previously (35), and Alexa Fluor® 568 dye were excited using 543-nm laser light from a helium-neon (HeNe) laser source, and emitted fluorescent light was filtered using a 585-nm long pass filter. Alexa Fluor 488 dye and EGFP were excited using a 488-nm laser line from an argon-krypton laser, and the emitted light was filtered using a long pass 505–530-nm barrier filter. Image processing was performed with ImageJ (National Institutes of Health).

**JHC 1-64 Live Cell Imaging**—NET surface expression was visualized in live SCG neurons grown on glial monolayers in LabTek chambers using the rhodamine-conjugated cocaine analogue JHC 1-64 (50 nM) in imaging buffer for 20 min at 4 °C to label surface NET. Subsequently, the buffer was removed, and the cells were rapidly washed twice with cold imaging buffer and imaged immediately using a Zeiss LSM 510 instrument. To verify the specific binding of JHC 1-64 to NET, some specimens were preincubated with desipramine (100  $\mu$ M) for 20 min before labeling with JHC 1-64. To visualize NET internalization in live neurons, SCG neurons were first incubated with JHC 1-64 (50 nM) at 4 °C to label surface NET. Subsequently, the buffer was removed and replaced with prewarmed imaging buffer, and internalization was allowed for 1 h at 37 °C. JHC 1-64-labeled NET was then visualized by confocal microscopy carried out at 37 °C. To assess the effect of activation of PKC on NET internalization, SCG neurons were incubated for 1 h at 37 °C in the presence of 1  $\mu$ M phorbol 12-myristate 13-acetate (PMA) or vehicle (0.01% DMSO) after surface labeling of NET with JHC 1-64 at 4 °C.

To investigate the postendocytic fate of internalized NET in live neurons, SCG neurons were transduced with different endosomal markers (EGFP-Rab4, -Rab7, -Rab11, and -Rab11 S25N) on days 4–5 *in vitro*. Next, transduced (and non-transduced) SCG neurons were incubated with JHC 1-64 (50 nM) to label surface NET before 1 h of internalization at 37 °C. After incubation, the living neurons were imaged by confocal microscopy carried out at 37 °C. To further assess the postendocytic fate of NET, we also visualized lysosomes by incubating non-transduced SCG neurons with LysoTracker Green (50 nM; Invitrogen) during the last 15 min of incubation at 37 °C. Finally, cells were washed twice and imaged at 37 °C.

**Antibody Feeding Assay (Internalization Assay)**—CAD cells transiently transfected with equal amounts of TacNET and EGFP-Rab7 or EGFP-Rab11 were seeded on coverslips treated with poly-L-ornithine. The cells were incubated with a mouse anti-FLAG antibody (M1 antibody) (1  $\mu$ g/ml) in DMEM at 4 °C for 30 min to label surface-expressed TacNET. Subsequently, cells were washed three times with DMEM and then incubated in prewarmed medium for 1 h at 37 °C allowing internalization (or at 4 °C as a non-trafficking surface control). Internalization was terminated by washing the cells with ice-cold PBS, followed by fixation in 4% paraformaldehyde at 4 °C for 20 min, permeabilization in blocking/permeabilization buffer, and incubation with anti-mouse Alexa Fluor 568 secondary antibody for 30 min. Finally, the specimens were washed, mounted in ProLong Gold Antifade reagent (Molecular Probes, Invitrogen), and visualized by confocal microscopy.

**Colocalization Assay**—To evaluate colocalization of the transporters with different endosomal markers, CAD cells were transiently transfected with equal amounts of the transporters of interest (NET, DAT, or NET-DAT chimeras) and either EGFP-Rab7 or EGFP-Rab11. JHC 1-64 internalization assays were performed 48 h post-transfection by labeling surface expressed transporters at 4 °C with JHC 1-64 (50 nM). Subsequently, the cells were incubated for 1 h at 37 °C to allow internalization and imaged at 37 °C. Evaluation of transporter colocalization with EGFP-Rab7 and EGFP-Rab11 was performed



with the investigator kept unaware of the molecular species under investigation.

**Quantification of Internalization**—Quantification of the fraction of internalized NET in live SCG neurons was performed from single confocal sections. Background subtraction was performed by setting a minimum threshold pixel intensity of 50 in the 8-bit pictures, to ensure that only specific JHC 1-64 signal contributed to the quantification. The entire neuronal somata and proximal extensions (ROI-total) and the cytoplasmic parts of the somata and proximal extensions (ROI-internalized) were manually selected from each image. Internalization was defined as the ratio of the total integrated density of internalized NET (ROI-internalized) and the total integrated density of the entire labeled NET pool (ROI-total). 20–29 cells from at least three independent experiments were used for quantification under each condition. Statistical analyses were performed with GraphPad Prism<sup>TM</sup>, and significance was determined using one-way ANOVA with Bonferroni's multiple-comparison test. Differences were considered significant when  $p$  was  $<0.05$ .

**Quantification of Colocalization**—Quantification of colocalization of NET, DAT, and NET-DAT chimeras with EGFP-Rab7 and EGFP-Rab11 was done using the Van Steensel's cross-correlation function in the JaCoP Plug-in for ImageJ as described before (36–38). Van Steensel's cross-correlation function reports the Pearson cross-correlation as a function of the relative movement of the two channels with respect to each other. Masks for the red and green channel were created using permanent settings for each image to avoid background. In a given overlay of the two images, the Pearson coefficient was plotted as a function of a 20-pixel shift in each  $x$  direction of one of the images compared with the other. According to the cross-correlation function, complete colocalization results in a cross-correlation function of 1 at  $Dx = 0$ , and mutually exclusive structures will tend to show no peak or even a dip at  $Dx = 0$ . Colocalization was quantified for 10–25 cells from three to five independent experiments. Results are means  $\pm$  S.E.

**Quantification of Distances from the Plasma Membrane of JHC 1-64/DAT- Versus JHC 1-64/NET-positive Vesicles**—Quantification of the distance of the JHC 1-64 positive vesicles from the plasma membrane in CAD cells transiently expressing NET or DAT was done using ImageJ. The distance from the plasma membrane was measured using the straight tool for 8–12 of the brightest JHC 1-64-positive vesicles per cell in 25–28 cells deriving from at least three independent transfections. Statistical significance was determined using an unpaired  $t$  test. Differences were considered significant when  $p$  was  $<0.05$ .

**Surface ELISA**—To evaluate changes in surface expression of NET upon prolonged incubation with JHC 1-64 or PMA, HEK cells transiently expressing FLAG-tagged TacNET were seeded on 96-well plates. 48 h post-transfection, the TacNET-expressing cells were incubated with 500 nM JHC 1-64, 1  $\mu$ M PMA, or vehicle (0.01% DMSO) for 1 h at 37 °C. Subsequently, the cells were washed with cold PBS, fixed in 4% paraformaldehyde, and blocked with 5% goat serum in PBS for 1 h at room temperature. The cells were incubated with 1  $\mu$ g/ml M1 antibody for 1 h in blocking buffer, washed four times with PBS, and incubated

with HRP-conjugated goat anti-mouse antibody (1:1000) in blocking buffer for 30 min at room temperature. Subsequently, the cells were washed four times with PBS and incubated with SuperSignal ELISA Femto Maximum Sensitivity Substrate (Pierce) for 30 s with shaking before luminescence was detected on a POLARstar Omega (BMG Labtech, Ortenberg, Germany) instrument. Results are presented as ratios of the surface signal from JHC 1-64- and PMA-treated cells relative to the surface signal from vehicle-treated cells on the same plate. Statistical significance was determined using a one-way ANOVA with Bonferroni's multiple-comparison test. Differences were considered significant when  $p$  was  $<0.05$ .

**Reversible Biotinylation (Internalization Assay)**—Reversible biotinylation experiments were performed using a protocol modified from Schramm and Limbird (39). CAD cells were transiently transfected with equal amounts of NET, DAT, and NET-DAT chimeras 48 h before the experiments. The cells were rapidly cooled by washing with cold PBS and surface-biotinylated with 1.2 mg/ml disulfide-cleavable biotin (sulfo-NHS-SS-biotin; Pierce) for 1 h on ice. Free biotin reagent was removed by quenching with glycine (100 mM) followed by two washes with PBS. Transporter endocytosis was initiated by incubating the cells with prewarmed medium with no extra treatment, leupeptin (100  $\mu$ g/ml), or leupeptin (100  $\mu$ g/ml) and monensin (25  $\mu$ M) for 1 h at 37 °C. Control plates were kept on ice to prevent internalization. To stop endocytosis and to dissociate the biotin from the cell surface-resident proteins, the cells were washed with cold medium and incubated two times for 20 min with cold MesNa (100 mM) in 50 mM Tris-HCl (pH 8.8), 100 mM NaCl, 1 mM EDTA, 0.2% BSA on ice and subsequently washed twice with cold PBS. To determine total biotinylation, a sample of biotinylated cells was not subjected to reduction with MesNa. Cells were lysed in lysis buffer (25 mM Tris, pH 7.5, 100 mM NaCl, 1 mM EDTA, 1% Triton X-100, 0.2 mM PMSF, 1 protease inhibitor mixture tablet (Roche Applied Science) per 25 ml of buffer and 5 mM *N*-ethylmaleimide) and centrifuged, and supernatants were collected. Total fractions were collected from all samples and mixed with an equal volume of 2 $\times$  loading buffer containing 1% SDS, 2.5%  $\beta$ -mercapthoethanol, and 100 mM dithiothreitol (DTT). For pull-down of the biotinylated proteins, the samples were incubated overnight with avidin beads (Pierce) at 4 °C under constant rotation. Beads were washed four times in lysis buffer, and bound proteins were eluted with 2 $\times$  loading buffer. Proteins were separated by SDS-PAGE and immunoblotted (primary antibodies used: anti-hNET (1:1000) (NET 17–01; Mab-Technologies) to detect wild-type NET; anti-hDAT (1:1000) (Mab369; Millipore) to detect DAT(1–59)/NET; polyclonal anti-DAT (1:500) (Santa Cruz Biotechnology) to detect wild-type DAT and NET(1–128)/DAT; and HRP-conjugated anti- $\beta$ -actin (1:10 000) (Sigma) in 5% milk powder in PBS plus 0.05% Tween; secondary antibodies used: HRP-conjugated anti-mouse, HRP-conjugated anti-rat and HRP-conjugated anti-goat (all 1:1000) (Pierce) in 5% milk powder in PBS plus 0.05% Tween). To estimate the relative amounts of transporters present in the blots, the transporter bands were scanned, and the band densities were quantified with ImageJ software.

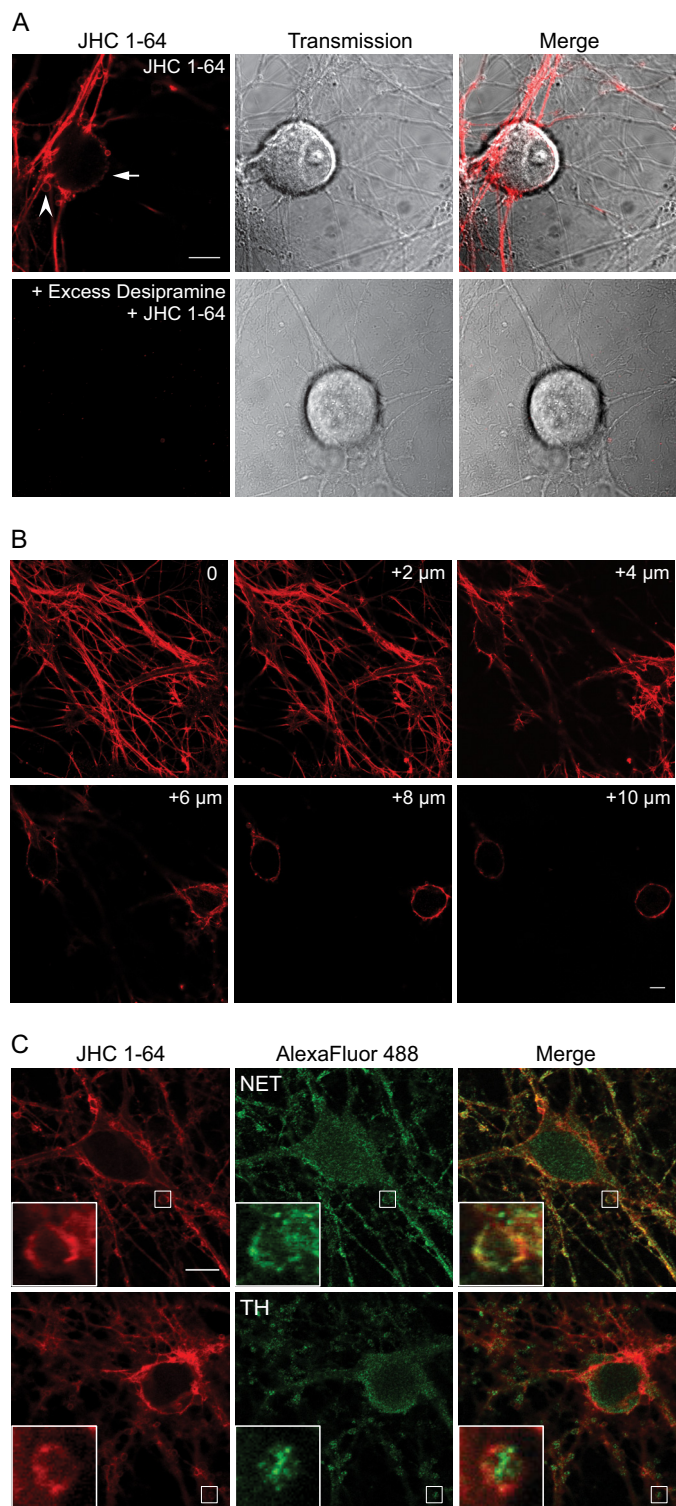


**FIGURE 1. Visualization of endogenously expressed NET in live cultured sympathetic neurons using the fluorescent cocaine analogue JHC 1-64.** A, labeling of JHC 1-64 is blocked by the NET inhibitor desipramine (100 μM). The SCG neurons were incubated with 50 nM JHC 1-64 (top) or preincubated with 100 μM desipramine (bottom) for 20 min before incubation for 20 min with 50 nM JHC 1-64. The experiments shown are representative of at least three similar experiments with the same results. Scale bar, 10 μm. B, z-scan of JHC 1-64-labeled SCG neurons. The scan demonstrates uniform surface distribution of NET in the axonal network, boutons, and somata. The pictures represent single confocal sections starting from the bottom of the neurite tree (0) and ending on 10 μm above the surface, on the level of the neuronal somas. The neuronal cultures were incubated with 50 nM JHC 1-64 before the analysis was performed. C, JHC 1-64 labels SCG neurons immunopositive for

## Results

**JHC 1-64 Enables Specific Labeling of Endogenous NET in SCG Neurons**—We first assessed whether the fluorescent cocaine analogue, JHC 1-64, could be used as a tool to specifically label surface-resident NET in primary neurons. JHC 1-64 contains a rhodamine moiety, extending from the tropane nitrogen of the parent compound 2β-carbomethoxy-3β-(3,4-dichlorophenyl)tropane with an ethylamino linker (35). We have previously used JHC 1-64 to visualize cell surface expression and internalization of both DAT and SERT (20, 22, 24, 35). Importantly, JHC 1-64 also displays high affinity for NET, as reflected by the potency by which JHC 1-64 inhibits [<sup>3</sup>H]dopamine uptake in NET-expressing cells ( $K_i \sim 194$  nM) (35). To test whether JHC 1-64 allowed labeling for native NET, we prepared primary cultures of sympathetic SCG neurons known to express high levels of NET (30). These neurons are characterized by large round somata and a very extensive network of neuronal projections with multiple “boutons” probably representing presynaptic NE release sites (40). Labeling of the neurons with 50 nM JHC 1-64, followed by confocal live imaging, revealed a strong fluorescent signal in the rhodamine channel (>585 nm) corresponding to the plasma membrane of the somata (arrow in Fig. 1A) as well as of the neuronal projections and the boutons (Fig. 1A, arrowhead). In general, JHC 1-64 labeling demonstrated the strongest intensity on the plasma membrane of the neuronal projections and the boutons. Consistent with specific visualization of NET, no labeling was observed of the glial cell layer, and preincubation with the NET inhibitor desipramine (100 μM) eliminated essentially all neuronal labeling (a typical SCG neuron is shown in Fig. 1A). The uniform and wide distribution of JHC 1-64-labeled NET in the SCG neurons is further illustrated by the z-scan through live noradrenergic neurons shown in Fig. 1B. The z-scan also highlights the presence of NET in the plasma membrane of the neuronal somata. Notably, NET expression in the plasma membrane of the somata has not been reported in previous studies (16, 40, 41). Taken together, the results suggest that JHC 1-64 efficiently labels endogenous NET in cultured noradrenergic neurons with high signal/noise ratio.

To substantiate that the neurons labeled with JHC 1-64 possessed features of noradrenergic neurons, we co-stained JHC 1-64-labeled SCG neurons with antibodies directed against noradrenergic cell markers. JHC 1-64 labeling was maintained in the fixed and permeabilized neurons, although the staining observed was somewhat weaker and more punctuated compared with live neurons, which most likely can be ascribed to the fixation and permeabilization procedure. JHC 1-64 labeling

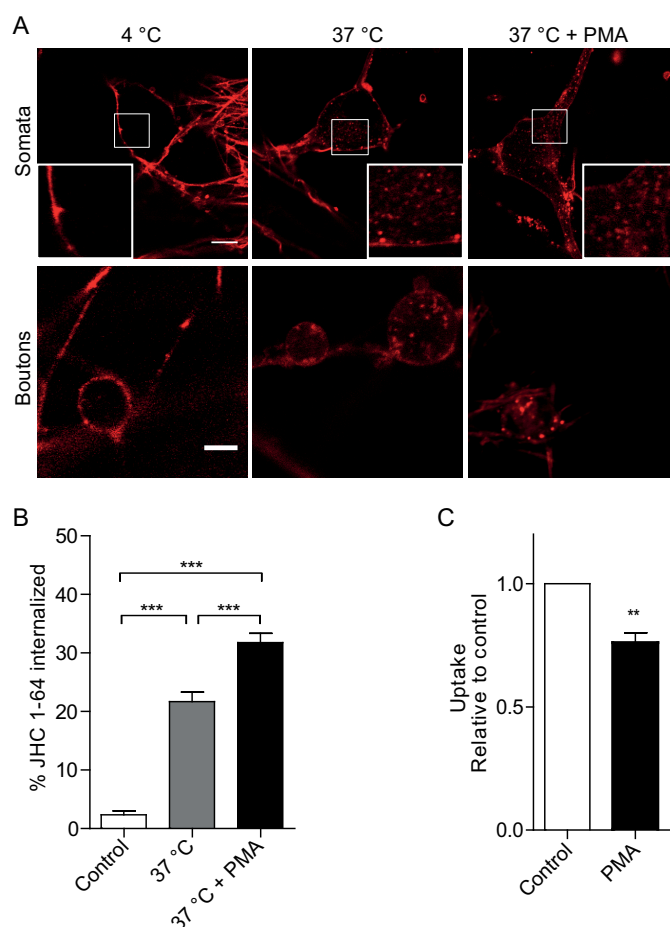
NET and tyrosine hydroxylase (TH). Cultured SCG neurons were labeled with 50 nM JHC 1-64 for 20 min before neurons were fixed, permeabilized, and stained with antibodies against the noradrenergic cell marker NET (top) or tyrosine hydroxylase (bottom). Costaining of SCG neurons with JHC 1-64 and mouse anti-NET antibody showed extensive overlap in the extensions and in the plasma membrane of the soma as well as the boutons. Costaining of SCG neurons with JHC 1-64 and anti-tyrosine hydroxylase antibody showed labeling of same cells but no direct overlap because the majority of tyrosine hydroxylase staining appeared intracellular. The experiments shown are representative of at least three similar experiments with the same results. The small white squares mark areas that are shown enlarged inside large squares. Scale bar, 10 μm.



was detected in the plasma membrane of the somata as well as the boutons of all neurons positive for NET immunoreactivity (Fig. 1C, top). Of note, the NET antibody also revealed considerable intracellular immunostaining corresponding to both somata and boutons (Fig. 1C, top). Finally, we found strong surface labeling with JHC 1-64 of tyrosine hydroxylase-positive neurons (Fig. 1C, bottom). The tyrosine hydroxylase immunoreactivity did not overlay with signal of JHC 1-64, because tyrosine hydroxylase staining appeared intracellular both in the somata and boutons.

**NET Is Constitutively Internalized in SCG Neurons and Phorbol Esters Increase Internalization**—To determine whether NET undergoes constitutive endocytosis in noradrenergic neurons, surface-expressed NET was labeled with 50 nM JHC 1-64 at 4 °C followed by incubation at 37 °C for 1 h to allow for internalization. Consistent with marked constitutive internalization of NET, confocal live imaging revealed accumulation of multiple JHC 1-64-positive intracellular vesicular structures that were not seen in cells kept at 4 °C (Fig. 2A). Internalized, JHC 1-64-labeled NET was found not only in the somata and proximal extensions but was also clearly visible in the cytoplasm of the boutons (Fig. 2A). Indeed, quantification of confocal sections of live SCG neurons showed significantly higher internalization of JHC 1-64-labeled NET upon incubation at 37 °C (constitutive internalization) compared with the 4 °C control (Fig. 2B). The intracellular accumulation of JHC 1-64-labeled NET was further enhanced upon incubation with the phorbol ester PMA, which activates protein kinase C as well as other kinases (11, 13, 14, 42) (Fig. 2A). Quantification of single sections demonstrated that PMA treatment significantly increased the amount of intracellular JHC 1-64-labeled NET (Fig. 2B). This finding was supported by [<sup>3</sup>H]dopamine uptake experiments demonstrating significant decreases in NET uptake capacity in response to PMA, compared with vehicle-treated SCG neurons (Fig. 2C).

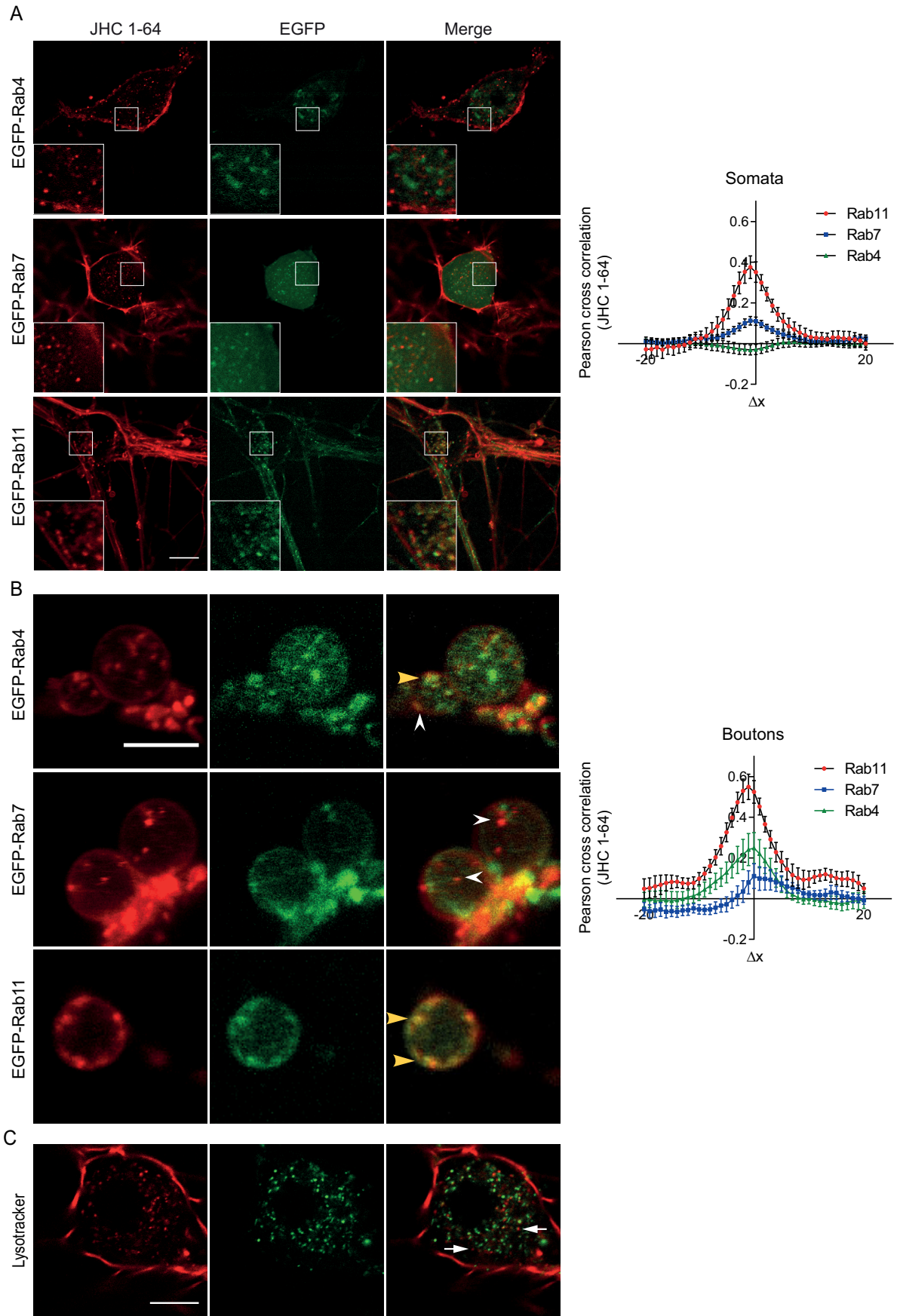
**Internalized NET Colocalizes with Rab11-positive Recycling Endosomes and Inhibition of Rab11 Attenuates NET Function**—To investigate the fate of internalized JHC 1-64-labeled NET, we transduced cultured SCG neurons with lentivirus encoding different endosomal markers tagged with EGFP (*i.e.* EGFP-Rab4, -Rab7, and -Rab11). High transduction efficiency was obtained, and the EGFP-tagged Rab proteins exhibited distinct cellular distribution in agreement with previous reports (43–45). In the transduced neurons, we observed similar clear intracellular accumulation of JHC 1-64-labeled NET after 1 h of incubation at 37 °C as in non-transduced neurons (Fig. 3, A and B). Imaging of the neurons revealed strikingly different colocalization patterns between the JHC 1-64-labeled NET and the individual Rab proteins. In the somata and proximal extensions, EGFP-Rab4, a marker of early endosomes and the “short loop” recycling pathway, was present in vesicular structures that showed very little overlap with internalized JHC 1-64-labeled NET (Fig. 3A). Similarly, we observed rather scant overlap between JHC 1-64-labeled NET and the vesicular structures to which the fluorescent signals from EGFP-Rab7, a marker of late endosomes, were localized (Fig. 3A). In contrast, the overlap between JHC 1-64-labeled NET and the signal from EGFP-Rab11, which marks the “long loop” recycling pathway, was



**FIGURE 2. Endogenous NET is constitutively internalized in SCG neurons, and internalization is increased by PMA.** A, confocal images of representative live SCG neurons demonstrating NET internalization in the somata (top) (scale bar, 10  $\mu$ m) and in the presynaptic boutons (bottom) (scale bar, 5  $\mu$ m) incubated under the indicated conditions. Surface-expressed NET was labeled by incubating the cultures with 50 nM JHC 1-64 for 20 min at 4 °C. Subsequently, the SCG neurons were imaged (4 °C), incubated at 37 °C for 1 h and imaged (37 °C), or incubated at 37 °C for 1 h in the presence of 1  $\mu$ M PMA and imaged (37 °C + PMA). JHC 1-64-labeled NET showed a higher degree of intracellular accumulation upon incubation at 37 °C (constitutive internalization) compared with cells kept at 4 °C. Moreover, the intracellular accumulation of JHC 1-64-labeled NET was further enhanced upon incubation with the phorbol ester PMA. The small white squares mark areas that are shown enlarged inside large squares. B, the quantification of the NET internalization in SCG neurons as outlined under “Experimental Procedures” shows significantly increased intracellular accumulation of JHC 1-64/NET vesicles during incubation at 37 °C for 1 h that is further enhanced in the presence of PMA (1  $\mu$ M) compared with cells kept at 4 °C. Data are means  $\pm$  S.E. (error bars), 23–29 cells,  $p < 0.001$ , one-way ANOVA, Bonferroni’s multiple-comparison test. C, [<sup>3</sup>H]dopamine uptake in cultured SCG neurons is significantly decreased in response to PMA (1  $\mu$ M) compared with vehicle-treated cells. [<sup>3</sup>H]Dopamine uptake was 746  $\pm$  60 and 1002  $\pm$  60 pmol/min/well, respectively. Data are means  $\pm$  S.E.,  $n = 5$ ,  $p < 0.01$ , one-sample *t* test.

strong (Fig. 3A). These observations were supported by quantification using Van Steensel’s cross-correlation analysis, in which the Pearson cross-correlation is calculated as the signal from one channel (*i.e.* JHC 1-64) is shifted relative to the signal from the other channel (*i.e.* EGFP) in the *x* direction pixel per pixel (36–38). The Pearson correlation was plotted as a function of a 20-pixel shift in each *x* direction of one of the images compared with the other. Consistent with strong colocalization of JHC 1-64-labeled NET with EGFP-Rab11, the cross-correlation function peaked at  $\Delta x \approx 0$  with a value of  $\sim 0.4$  (Fig. 3A).

# Internalization and Recycling of NET



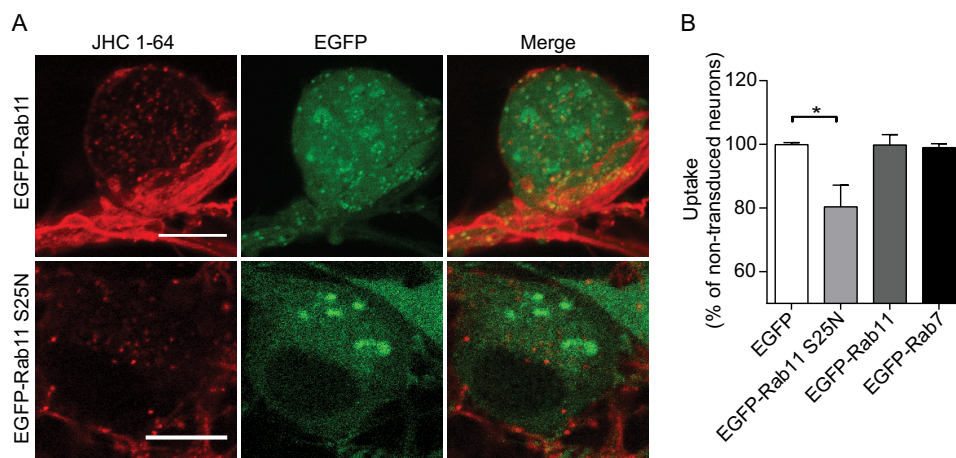


**FIGURE 4. Prolonged inhibition of Rab11 attenuates NET function.** *A*, postendocytic sorting of NET in SCG neurons transduced with lentivirus encoding EGFP-tagged wild-type Rab11 or dominant negative Rab11 (Rab11 S25N). The analysis was done by labeling surface-expressed NET with JHC 1-64 followed by internalization for 1 h at 37 °C. Subsequently, the live cells were imaged at 37 °C using an LSM 510 confocal microscope. Both panels show representative somata. Overexpression of the EGFP-Rab11 S25N compared with EGFP-Rab11 changed the morphology of the endocytic recycling compartment. Scale bar, 10  $\mu$ m. *B*, lentivirus-mediated transduction of Rab11 S25N resulted in a significant decrease in the [ $^3$ H]DA uptake rate compared with neurons overexpressing EGFP. Data are means  $\pm$  S.E. (error bars),  $n = 3-5$ ,  $p < 0.05$ , one-way ANOVA, Dunn's multiple-comparison test.

The peak value for EGFP-Rab7 was lower, and no peak was seen for EGFP-Rab4 (Fig. 3A).

In the boutons, we also observed strong overlap between internalized JHC 1-64-labeled NET and EGFP-Rab11-positive endosomes and little overlap with EGFP-Rab7 (Fig. 3B). Note that expression of EGFP-Rab7 is not unexpected in the axonal compartment, where Rab7 is believed to play a role in retrograde transport (46). For EGFP-Rab4, we interestingly observed an apparent higher degree of colocalization with internalized NET in the boutons compared with the somata and proximal extensions (Fig. 3B). Again, these findings were supported by cross-correlation analysis showing the highest peak value for EGFP-Rab11, hardly any peak for EGFP-Rab7, and a peak value of  $\sim 0.22$  for EGFP-Rab4 (Fig. 3B).

To further substantiate the distinct postendocytic fate of NET, we investigated the colocalization of internalized JHC 1-64-labeled NET with the lysosomal marker LysoTracker that has previously been shown to colocalize with constitutively internalized DAT and SERT (22, 24, 49). Consistent with sorting to a recycling pathway and not to degradation, we observed by live confocal imaging limited colocalization of internalized JHC 1-64-labeled NET with LysoTracker (Fig. 3C).

In light of the robust constitutive internalization, the localization of internalized NET to Rab11-positive endosomes sug-

gests that recycling of NET via the long loop recycling pathway might be critical for maintenance of steady state NET surface levels and consequently NET function. To assess this, we mitigated the function of the Rab11 compartment by overexpressing the dominant negative Rab11 mutant, Rab11 S25N. Rab11 S25N mimics the GDP-bound, inactive form of Rab11 and is commonly used to inhibit Rab11-mediated recycling (16, 50–54). It has been shown that Rab11 S25N can significantly change the morphology of endocytic recycling endosomes and decrease their colocalization with cargo (54). Indeed, we observed a prominent change in the localization of recycling endosomes upon expression of Rab11 S25N (*i.e.* the disrupted recycling endocytic compartment was localized more peripherally and was dispersed) (compare EGFP-Rab11 with EGFP-Rab11 S25N in Fig. 4A). The overexpression of EGFP-Rab11 S25N resulted moreover in a significant decrease in NET transport capacity compared with neurons only overexpressing EGFP, as illustrated by reduced [ $^3$ H]DA uptake (Fig. 4B). Overexpression of EGFP-Rab11, as well as of EGFP-Rab7, did not alter NET transport capacity (Fig. 4B). A role of the Rab11 pathway was further supported by experiments in transfected CAD cells, where co-expression of NET with Rab11 S25N, caused a significant decrease in [ $^3$ H]DA uptake ( $V_{\max} = 72 \pm 6\%$  of control (mean  $\pm$  S.E.),  $n = 4$ ) compared with cells co-express-

**FIGURE 3. Internalized NET is primarily sorted to Rab11-positive recycling endosomes.** SCG neurons were transduced with lentivirus encoding EGFP-Rab4, -Rab7, or -Rab11 at 4–5 days *in vitro*. The analysis of postendocytic sorting of NET was performed after 8–11 days *in vitro* by labeling surface-expressed NET with JHC 1-64 and allowing for internalization for 1 h at 37 °C. Subsequently, the live cells were analyzed at 37 °C by confocal imaging. *A*, left, confocal live images of internalized JHC 1-64-labeled NET in neuronal somata showing colocalization with EGFP-Rab11-positive endosomes and limited association with EGFP-Rab4 and EGFP-Rab7 positive endosomes. Scale bar, 10  $\mu$ m. Right, quantification of colocalization between internalized JHC 1-64-labeled NET and EGFP-tagged endosomal markers in neuronal somata using Van Steensel's cross-correlation function that reports the Pearson cross-correlation as a function of the relative movement of the two channels with respect to each other. The data support strong colocalization of internalized JHC 1-64-labeled NET with EGFP-Rab11, less colocalization with EGFP-Rab7, and no colocalization with EGFP-Rab4 (see "Experimental Procedures" for further details). *B*, left, confocal live images of internalized JHC 1-64-labeled NET in boutons of SCG neurons showing colocalization with EGFP-Rab11-positive endosomes, some colocalization with EGFP-Rab4-positive endosomes, and limited association with EGFP-Rab7-positive endosomes. Yellow arrowheads, examples of colocalized vesicles. White arrowheads, examples of non-colocalized vesicles. Scale bar, 5  $\mu$ m. Images are representative of at least three independent experiments. Right, quantification of colocalization using Van Steensel's cross-correlation function. The data support strong colocalization of internalized JHC 1-64-labeled NET with EGFP-Rab11, some colocalization with EGFP-Rab4, and little colocalization with EGFP-Rab7 (see "Experimental Procedures" for further details). *C*, constitutively internalized NET demonstrates little colocalization with the lysosomal marker, LysoTracker Green. SCG neurons labeled with JHC 1-64 were incubated with LysoTracker Green during the last 15 min of the internalization period (1 h) at 37 °C, and the live cells were imaged at 37 °C using an LSM 510 confocal microscope. Scale bar, 10  $\mu$ m. Images are representative of at least three independent experiments.



## Internalization and Recycling of NET

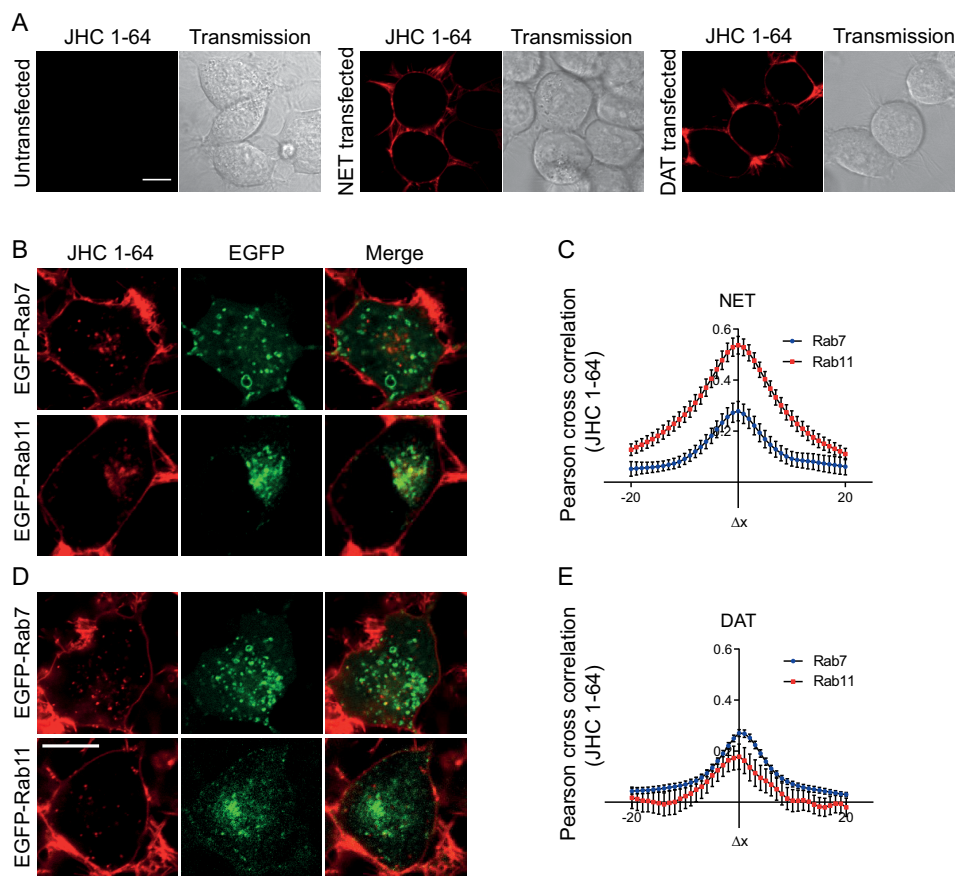


**FIGURE 5. NET and DAT have distinct postendocytic fate in transfected CAD cells.** *A*, confocal live cell images and corresponding transmission images of untransfected CAD cells (*left*), cells transiently expressing NET (*middle*), or cells transiently expressing DAT (*right*). Cells were incubated with JHC 1-64 (50 nM) for 20 min at 4 °C before imaging. *Scale bar*, 10  $\mu$ m. *B*, confocal live microscopy images of internalized JHC 1-64-labeled NET exhibiting strong colocalization with EGFP-Rab11-positive endosomes and limited association with EGFP-Rab7-positive endosomes. *C*, confocal live microscopy images of internalized JHC 1-64-labeled DAT exhibiting limited colocalization with EGFP-Rab11-positive endosomes and stronger association with EGFP-Rab7-positive endosomes. *Scale bar*, 10  $\mu$ m. *D*, quantification of colocalization using Van Steensel's cross-correlation function. The data support the strongest colocalization of internalized JHC 1-64-labeled NET with EGFP-Rab7 and less colocalization with EGFP-Rab11 (see "Experimental Procedures" for further details). *E*, quantification of colocalization using Van Steensel's cross-correlation function. The data support the strongest colocalization of internalized JHC 1-64-labeled NET with EGFP-Rab7 and less colocalization with EGFP-Rab11 (see "Experimental Procedures" for further details). *Error bars*, S.E.

ing NET and wild-type Rab11. Co-expression of NET with dominant negative Rab4 (Rab4 S25N), however, did not cause any change in NET uptake rate compared with the cells expressing wild-type Rab 4 ( $V_{\max} = 100 \pm 9\%$  of control (mean  $\pm$  S.E.),  $n = 3$ ). Altogether, our results suggest that to a major extent, constitutively internalized NET is sorted to the Rab11 recycling compartment in SCG neurons and that impairment of the Rab11 pathway results in decreased NET function.

**NET and DAT Have Distinct Trafficking Properties**—We have recently characterized in detail the postendocytic fate of constitutively internalized DAT and SERT, which both appeared to be sorted largely to late endosomes and lysosomal degradation (21, 22). Thus, we did not expect that constitutively internalized NET would be sorted primarily to the Rab11 recycling compartment in primary neurons. To further characterize the fate of NET, we wanted to directly compare NET with DAT; therefore, we turned to a heterologous expression system. To distinguish between the Rab11 recycling compartment and the Rab7 late endosomal compartment, NET and DAT were transiently transfected into catecholaminergic CAD cells (55, 56). Importantly, we observed no background labeling of these cells with JHC 1-64 (Fig. 5A). In contrast, we observed strong plasma

membrane labeling of CAD cells transiently expressing either NET or DAT (Fig. 5A). Next, we co-expressed NET or DAT with either EGFP-Rab7 or EGFP-Rab11. The cells were labeled with JHC 1-64, followed by incubation at 37 °C for 1 h to allow constitutive internalization. Similarly to our findings in noreadrenergic neurons, we observed strong JHC 1-64 labeling of the plasma membrane in NET expressing CAD cells. Moreover, we observed accumulation of multiple intracellular JHC 1-64-positive vesicles during the 37 °C internalization period, consistent with constitutive internalization. Such vesicular structures were not observed in cells kept at 4 °C, and no labeling or accumulation of JHC 1-64 were seen in the presence of the NET inhibitor desipramine (data not shown). Importantly, internalized, JHC 1-64-labeled NET colocalized prominently with EGFP-Rab11 but only to a limited extent with EGFP-Rab7 (Fig. 5A). This was supported by cross-correlation analysis indicating marked colocalization with EGFP-Rab11 and less with EGFP-Rab7 (Fig. 5B). In agreement with our previous findings for DAT (24), we also observed strong JHC 1-64 labeling of DAT-expressing CAD cells and intracellular accumulation of JHC 1-64-labeled DAT upon incubation at 37 °C (Fig. 5C). Internalized JHC 1-64-labeled DAT, however, showed substan-

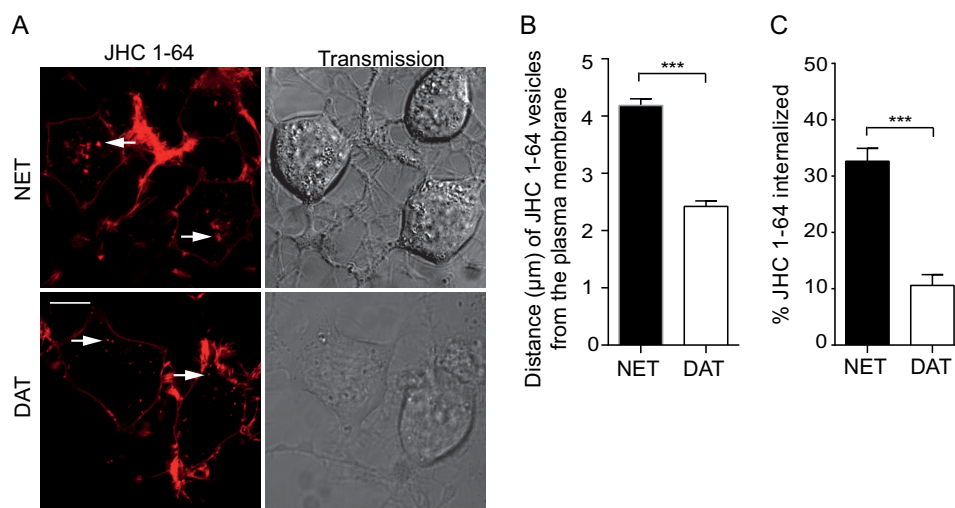


**FIGURE 6. NET displays higher degree of constitutive internalization than DAT in transiently transfected CAD cells.** *A*, representative confocal live images of JHC 1-64 labeled internalized NET (*top left*) and DAT (*bottom left*). Corresponding transmission images are shown in the *right panels*. For the experiments, surface-expressed transporter were labeled with JHC 1-64 and allowed to internalize for 1 h at 37 °C. Subsequently, the live cells were imaged at 37 °C using an LSM 510 confocal microscope. Quantification of the internalization of JHC 1-64 was performed as described under "Experimental Procedures." Scale bar, 10  $\mu\text{m}$ . *B*, quantification of the distance from the plasma membrane to JHC 1-64-labeled NET-positive vesicles compared with JHC 1-64-labeled DAT-positive vesicles. JHC 1-64/NET-positive vesicles display in the CAD cells a significantly more perinuclear localization compared with internalized JHC 1-64/DAT-positive vesicles. Examples are indicated by *white arrows*. Quantification of the JHC 1-64 vesicle distances were performed as described under "Experimental Procedures." Data are means  $\pm$  S.E. (*error bars*),  $n = 25\text{--}28$  cells from at least three independent experiments,  $p < 0.001$ , *t* test. *C*, quantification of internalization revealed significantly higher internalization of JHC 1-64-labeled NET compared with DAT. Data are means  $\pm$  S.E.,  $n = 62\text{--}75$  cells from five independent experiments,  $p < 0.001$ , *t* test.

tially less colocalization with EGFP-Rab11 compared with JHC 1-64-labeled NET (Fig. 5, *C* and *D*). Instead, JHC 1-64-labeled DAT appeared to be more associated with EGFP-Rab7 (Fig. 5, *C* and *D*).

Interestingly, and further supporting a differential sorting pattern, internalized NET-positive vesicles seemed to have a more perinuclear localization compared with internalized DAT vesicles, which showed more peripherally located puncta (Fig. 6*A*). To assess the differential localization of JHC 1-64-labeled NET and DAT vesicles, we measured the closest distance of 8–12 of the brightest vesicles per cell to the plasma membrane in 25–28 cells deriving from at least three independent transfections. Interestingly, JHC 1-64/DAT vesicles were significantly closer to the plasma membrane compared with NET/JHC 1-64 vesicles that appeared more perinuclear ( $2.4 \pm 0.1 \mu\text{m}$  (DAT) *versus*  $4.2 \pm 1.2 \mu\text{m}$  (NET) (means  $\pm$  S.E.)) (Fig. 6*B*). Moreover, our images indicated that the constitutive NET internalization was more intense compared the DAT internalization. We quantified accordingly the fraction of JHC 1-64-labeled NET and DAT, which confirmed that a significantly higher fraction of NET was internalized compared with DAT in CAD cells transiently expressing NET and DAT (Fig. 6*C*).

**Internalized TacNET Colocalizes with Rab11 Endosomes—**We showed previously that JHC 1-64 has a very slow off-rate from DAT, making it a reliable marker of DAT trafficking (20). To assess whether the off-rate from NET likewise was slow, we used a procedure similar to the one that we used previously for DAT (20). We assessed the capability of JHC 1-64 to inhibit [ $^3\text{H}$ ]DA uptake in NET-expressing CAD cells upon prolonged incubation and wash-outs to permit dissociation and preclude reassociation of JHC 1-64. The cells were incubated with 500 nM JHC 1-64 or vehicle for 30 min, followed by washing and incubation for 0, 20, 40, 60, or 90 min at 37 °C. After two addi-

tional washes, [ $^3\text{H}$ ]DA uptake was measured, and we found that uptake was still inhibited to almost the same extent ( $\sim 90\%$ ) as it was when measuring uptake with no washout immediately after the addition of 500 nM JHC 1-64 (data now shown). This strongly suggests that the off-rate of JHC 1-64 is very slow also from NET and that JHC 1-64 therefore should be a reliable tool for tracking both NET and DAT in live cells even over extended time periods.

We wanted subsequently to exclude the possibility that binding of JHC 1-64 to the transporter affects the internalization and postendocytic sorting properties of NET described above. We therefore generated a fusion construct where the intracellular C terminus of the single transmembrane segment protein Tac was fused to the intracellular N terminus of NET (Fig. 7*A*). Because Tac contains an N-terminal M1 FLAG recognition sequence, we obtained in this way a transporter (TacNET) with an extracellular high affinity antibody epitope ideal for assaying internalization in antibody feeding experiments. Note that no high affinity antibody against an endogenous extracellular NET epitope is available. Previously, we have made similar constructs for DAT and SERT (TacDAT and TacSERT) that have proven very useful for studying the trafficking properties of these transporters (21, 22). Similar to TacDAT and TacSERT, TacNET exhibited clear functional activity, although its maximum uptake capacity was somewhat reduced as compared with wild-type NET ( $K_m = 0.30 \pm 0.06 \mu\text{M}$  for TacNET *versus*  $0.35 \pm 0.08 \mu\text{M}$  for wild-type NET,  $V_{\text{max}} = 23 \pm 5\%$  of wild-type NET (means  $\pm$  S.E.),  $n = 3$ ). For the antibody-based internalization assay, CAD cells expressing TacNET were first incubated with M1 antibody at 4 °C to label surface TacNET. Confocal imaging of the cells upon fixation (no permeabilization) and immunostaining with Alexa Fluor 568-conjugated secondary antibody revealed a fluorescent signal corresponding to the plasma



## Internalization and Recycling of NET

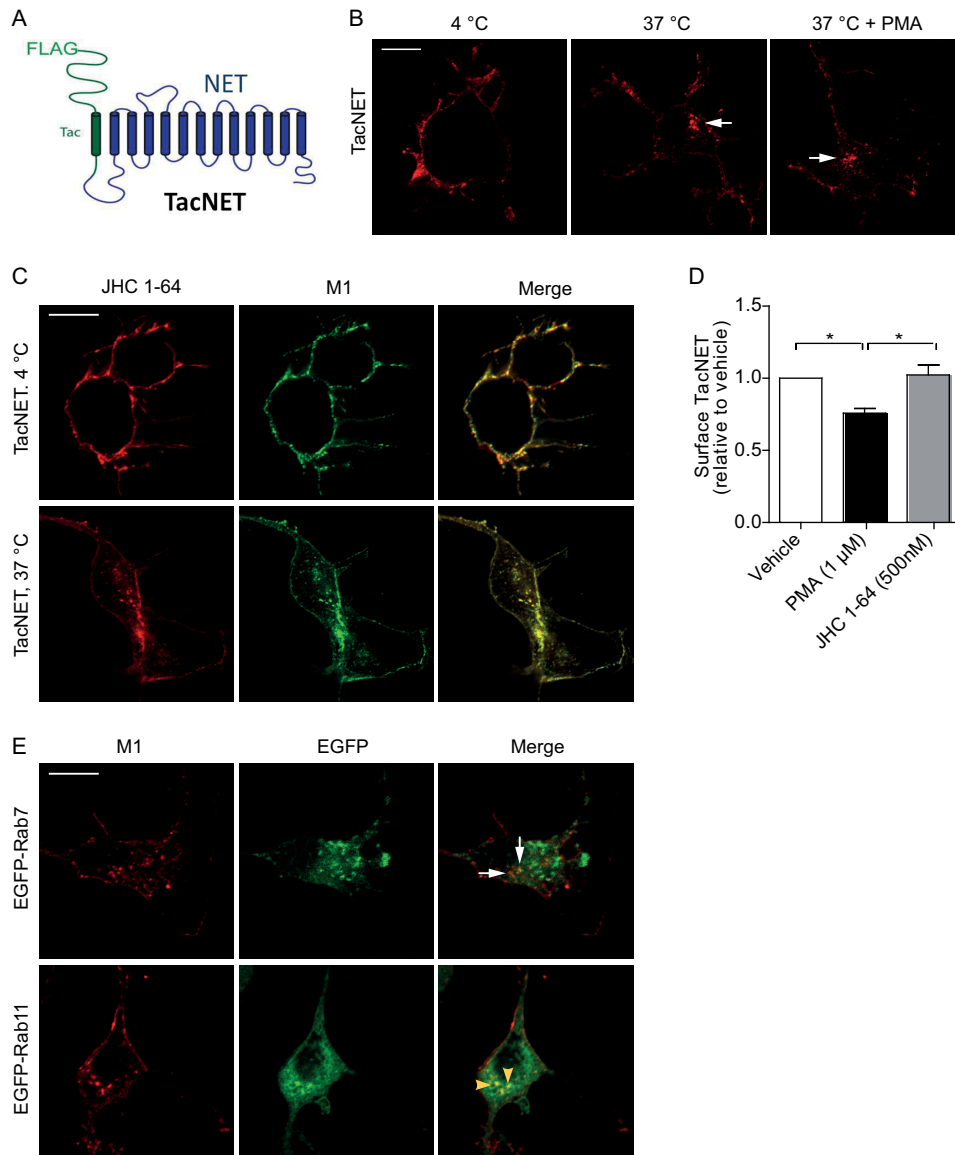


**FIGURE 7. Internalized TacNET is sorted to Rab11 positive recycling endosomes and surface expression is not affected by JHC 1-64.** *A*, schematic representation of TacNET where the single transmembrane protein Tac containing an N-terminal FLAG epitope was fused to the N terminus of NET. *B*, immunostainings without permeabilization of CAD cells transiently expressing TacNET using the M1 antibody recognizing the extracellular FLAG epitope. *Left*, 4 °C control showing plasma membrane expression of TacNET; *middle*, image obtained after 1 h of antibody feeding at 37 °C; *right*, image obtained after 1 h of antibody feeding at 37 °C in the presence of PMA (1  $\mu\text{M}$ ). The images suggest that TacNET undergoes marked constitutive internalization and that PMA increases this intracellular accumulation of the transporter. *Arrows*, internalized TacNET. *C*, visualization of surface-expressed TacNET (*top*) and TacNET internalization (*bottom*) using both M1 immunostaining with Alexa Fluor 488-conjugated secondary antibody and JHC 1-64 in CAD cells transiently expressing TacNET. First, the cells were incubated with JHC 1-64 for 20 min at 4 °C followed by incubation with the M1 antibody at 4 °C to label surface TacNET. TacNET internalization was visualized by labeling the surface-expressed TacNET with JHC 1-64 as well as with M1 antibody and the Alexa Fluor 488-conjugated secondary antibody and incubating the cells for 1 h at 37 °C. The fluorescent signals from the two different channels almost completely overlap. *D*, JHC 1-64 does not affect TacNET surface expression in HEK 293 cells. HEK 293 cells transfected with TacNET were incubated with PMA (1  $\mu\text{M}$ ), JHC 1-64 (500 nM), or vehicle for 1 h at 37 °C before quantification of surface TacNET by ELISA as described under "Experimental Procedures." No significant difference in the TacNET surface levels were detected upon JHC 1-64 (500 nM) treatment compared with vehicle-treated cells, whereas PMA (1  $\mu\text{M}$ ) significantly decreased TacNET surface expression. Data are means  $\pm$  S.E. (*error bars*),  $n = 6$ ,  $p < 0.05$ , one-way ANOVA, Bonferroni's multiple-comparison test. *E*, constitutively internalized TacNET colocalizes with Rab11-positive recycling endosomes. Confocal microscopy images of colocalization between TacNET and EGFP-Rab7 and EGFP-Rab11 after 1 h of antibody feeding with M1 antibody at 37 °C. M1 antibody was visualized by Alexa Fluor 568-conjugated secondary antibody after cells were fixed and permeabilized. TacNET exhibits intensive colocalization with EGFP-Rab11 but little with Rab7. Data are representative images of at least three independent experiments. *Scale bars*, 10  $\mu\text{m}$ .

membrane, suggesting that TacNET was expressed at the cell surface (Fig. 7*B*). We then analyzed cells after 1 h at 37 °C and observed marked intracellular accumulation of TacNET immunosignal in vesicular structures, consistent with constitutive internalization (Fig. 7*B*) as was observed for the JHC 1-64-bound transporter. This accumulation appeared, as would be

expected, generally stronger upon treatment of the cells with PMA during the 1-h internalization period (Fig. 7*B*). We also performed experiments where we visualized surface TacNET using both M1 immunostaining with Alexa Fluor 488-conjugated secondary antibody and JHC 1-64 at the same time by incubating the cells with JHC 1-64 for 20 min at 4 °C prior to

incubation with the M1 antibody at 4 °C. In addition, we visualized TacNET internalization by labeling the surface-expressed TacNET with antibodies (M1 and Alexa Fluor 488-conjugated secondary antibody) and JHC 1-64 following internalization for 1 h at 37 °C. Importantly, the fluorescent signals from the two different channels almost completely overlapped (Fig. 7C).

The presence of the FLAG epitope in TacNET furthermore enabled the employment of an ELISA-based assay to quantify surface expression of the transporter (24). According to this assay, incubation of the cells for 1 h at 37 °C with PMA caused a significant decrease in TacNET surface expression (Fig. 7D), confirming our observations by confocal imaging that PMA indeed causes redistribution of TacNET away from the plasma membrane. In contrast, incubation of the cells with JHC 1-64 at a saturating concentration (500 nM) for the same period of time did not cause any change in TacNET surface expression (Fig. 7D). This indicates that JHC 1-64 does not by itself affect transporter trafficking.

To obtain evidence that labeling of the transporter with JHC 1-64 also did not affect the postendocytic fate of NET, we performed antibody-based internalization assays in CAD cells expressing TacNET together with either EGFP-Rab7 or EGFP-Rab11. Consistent with the live imaging of native NET, constitutively internalized M1-labeled TacNET exhibited extensive colocalization with EGFP-Rab11 and showed little colocalization with EGFP-Rab7 (Fig. 7E). Thus, our TacNET experiments suggest that JHC 1-64 labeling does not affect the basic trafficking properties of the transporter.

**Inhibition of Recycling Increases NET, but Not DAT, Intracellular Accumulation**—Next, we employed a biochemical internalization assay (reversible biotinylation) to further investigate the trafficking properties of NET and DAT independent of fluorescent confocal imaging. CAD cells expressing non-tagged NET were biotinylated, using the reducible biotinylation reagent sulfo-NHS-SS-biotin, whereupon internalization was permitted by incubating the cells at 37 °C for 1 h. By treating the cells with the reducing agent MesNa, biotin residing on the cell surface was removed, and subsequently, intracellular biotinylated proteins were isolated and analyzed by Western blotting. The results strongly supported extensive internalization of NET by revealing significantly stronger NET immunoreactivity for cells incubated at 37 °C for 1 h as compared with cells kept at 4 °C (Fig. 7A, lanes 2 and 3). Interestingly, inhibition of lysosomal degradation by the lysosomal protease inhibitor leupeptin during the internalization period did not cause any further increase in the amount of NET immunoreactivity and thus intracellular NET levels. However, additional inhibition of recycling by monensin, a cation ionophore blocking recycling (57), caused a significant increase in NET levels (Fig. 8A), supporting our results from the imaging experiments indicating that NET is primarily recycled and not targeted to degradation upon internalization.

Our confocal fluorescence imaging results were further supported by reversible biotinylation experiments performed on DAT-expressing CAD cells. The experiments showed that DAT undergoes constitutive internalization as well (*i.e.* we found stronger DAT immunoreactivity for cells incubated at

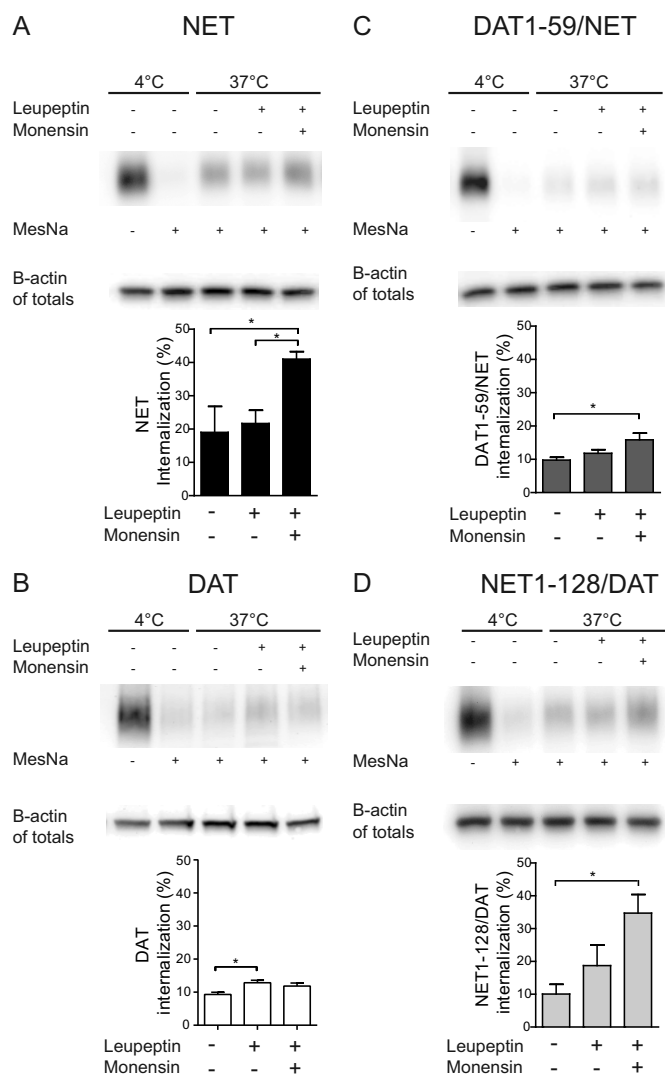


**FIGURE 8. Assessing internalization and postendocytic sorting of DAT, NET, and DAT/NET chimeras by reversible biotinylation experiments.** Shown is a reversible biotinylation (internalization) assay on CAD cells transiently expressing NET, DAT, DAT(1-59)/NET, or NET(1-128)/DAT. *Top panels*, lanes 1 and 2 from the left (4 °C) show total surface immunosignal (no stripping with MesNa) and after stripping (+MesNa). Lanes 3-5, accumulation of intracellular immunosignal after 1 h at 37 °C with no treatment, with inhibition of lysosomal degradation (leupeptin), and with inhibition of lysosomal degradation and recycling (leupeptin + monensin), respectively. *Bottom panels*, quantification of biotinylation data. *A*, intracellular accumulation of NET immunosignal (NET 17-01 antibody) was significantly increased in response to both leupeptin and monensin but not in response to leupeptin alone. *B*, intracellular accumulation of DAT immunosignal (DAT C-terminal antibody) was significantly increased in response to leupeptin with no further increase in response to both leupeptin and monensin. *C*, intracellular accumulation of DAT(1-59)/NET immunosignal (DAT antibody, Mab369) was significantly increased in response to both leupeptin and monensin but not in response to leupeptin alone; however, the apparent degree of internalization (with degradation and recycling blocked by leupeptin and monensin) was lower than of NET. *D*, intracellular accumulation of NET(1-128)/DAT immunosignal (DAT C-terminal antibody) was significantly increased in response to both leupeptin and monensin but not in response to leupeptin alone. Note that the apparent degree of internalization (with degradation and recycling blocked by leupeptin and monensin) was higher than that of DAT and more similar to NET. Data are means  $\pm$  S.E. (error bars),  $n = 3-5$ ,  $p < 0.05$ , one-way ANOVA, Bonferroni's multiple-comparison test.

37 °C for 1 h as compared with cells kept at 4 °C) (Fig. 8B, lanes 2 and 3). Importantly, we observed different effects of leupeptin and monensin on DAT as compared with NET; inhibition of



## Internalization and Recycling of NET

**TABLE 1**  
 **$K_m$  and  $V_{max}$  values for the wild-type and chimeric transporters**

The transport kinetics of dopamine were assessed in CAD cells transiently expressing wild-type and chimeric transporters. The  $K_m$  and  $V_{max}$  values were determined by nonlinear regression fits determined from 3–6 independent experiments performed in triplicates.  $K_m$  values are reported as the mean  $\pm$  S.E., and  $V_{max}$  values are expressed relative to NET (mean  $\pm$  S.D.).

Transporter	$K_m$	$V_{max}$
	$\mu M$	% of NET
DAT	$1.90 \pm 0.15$	$400 \pm 80$
NET	$0.46 \pm 0.12$	100
NET(1–128)/DAT	$0.64 \pm 0.05$	$230 \pm 48$
DAT/NET(590–617)	$1.90 \pm 0.40$	$310 \pm 44$
DAT(1–59)/NET	$1.18 \pm 0.58$	$156 \pm 19$
NET/DAT(591–620)	$0.48 \pm 0.13$	$96 \pm 9$

lysosomal degradation (leupeptin) showed a significantly increased intracellular accumulation of DAT, and additional inhibition of recycling (leupeptin and monensin) did not further increase the DAT immunosignal (Fig. 8B), in agreement with DAT being sorted to a larger degree to degradation than to recycling. It is also interesting to note that the apparent degree of internalization was lower for DAT compared with NET as determined with recycling and degradation blocked by leupeptin and monensin ( $12 \pm 1$  versus  $41 \pm 2\%$ , respectively,  $n = 3–4$ ; Fig. 8, compare A and B).

*The NET and DAT N Termini Are Critical for Internalization and Postendocytic Sorting*—Our findings suggest strikingly different trafficking itineraries for NET compared with DAT. To test whether specific NET or DAT domains encoded information sufficient to direct internalized transporter to specific endosomal compartments, we assessed the endocytic properties of chimeras between NET and DAT where the N and C termini were exchanged between the two proteins. All chimeras were readily expressed at the plasma membrane and exhibited normal functional activity (Table 1). In addition, all chimeras could be labeled with JHC 1-64, allowing us to perform single-cell internalization assays in CAD cells transiently expressing NET, DAT, NET/DAT(593–620), DAT(1–59)/NET, DAT/NET(590–617), or NET(1–128)/DAT together with EGFP-Rab7 or EGFP-Rab11. Surface-expressed transporters were labeled with JHC 1-64 (50 nM), internalized at 37 °C for 1 h, and colocalization of the internalized transporter with EGFP-Rab7 and EGFP-Rab11 was quantified from confocal images.

Introducing the DAT C terminus in NET (NET/DAT(593–620)) did not notably alter NET postendocytic fate, and thus the chimera colocalized mostly with EGFP-Rab11 and less with Rab7 (Fig. 9, A–C). In contrast, introducing the DAT N terminus into NET (DAT(1–59)/NET) profoundly decreased colocalization with EGFP-Rab11 without altering the colocalization with EGFP-Rab7 (Fig. 9, A–C). Correspondingly, introducing the NET C terminus into DAT (DAT/NET(590–617)) did not alter the postendocytic fate of the transporter (strongest colocalization with Rab7 and less with Rab11) (Fig. 9, D–F), whereas introducing the NET N terminus into DAT (NET(1–128)/DAT) markedly increased colocalization with EGFP-Rab11 without altering the colocalization with Rab7 (Fig. 9, D–F). Together, these results suggest that the differential sorting of NET and DAT is in part determined by non-conserved structural elements in the N termini of the transporters.

To further validate that the N terminus is critical for endocytosis and sorting of NET, we performed reversible biotinylation assays on the N-terminal chimeras. By introducing the DAT N terminus in NET (DAT(1–59)/NET), we observed internalization properties more similar to those seen for wild-type DAT. The apparent rate of internalization was lower at control conditions and, although there was still an increase in the DAT(1–59)/NET immunosignal when the cells were incubated with both leupeptin and monensin, the increase was more modest (Fig. 8C). As a result, the degree of internalization, as determined with recycling and degradation blocked by leupeptin and monensin, was higher for wild-type NET compared with DAT(1–59)/NET ( $41 \pm 2$  versus  $16 \pm 2\%$ , respectively,  $n = 3–4$ ) (Fig. 8, A and C). Similarly, by introducing the NET N terminus into DAT (NET(1–128)/DAT), we observed internalization properties more similar to those seen for wild-type NET. Blocking lysosomal degradation with leupeptin modestly increased NET(1–128)/DAT immunosignal, whereas additional blocking of recycling with monensin had a significant effect on NET(1–128)/DAT immunosignal compared with control conditions (37 °C, no treatment) (Fig. 8D). As a result, the degree of internalization, as determined with recycling and degradation blocked by leupeptin and monensin, was higher for NET(1–128)/DAT compared with wild-type DAT ( $32 \pm 8$  versus  $12 \pm 1\%$ , respectively (mean  $\pm$  S.E.),  $n = 3–4$ ) (Fig. 8, B and D).

## Discussion

Despite the physiological and pharmacological significance of NET, the cellular processes that control the trafficking of the transporter to and from the plasma membrane are still rather poorly understood. Here, we provide novel insight into the trafficking itinerary of NET by employing several different approaches. In particular, we take advantage of the fluorescent cocaine analogue JHC 1-64, which provides a powerful tool enabling direct visualization of surface distribution, internalization, and postendocytic sorting of endogenous NET even in single boutons of live neurons. Importantly, JHC 1-64 itself is unlikely to have any significant effect on NET trafficking. By using the TacNET construct, which adds an extracellular FLAG antibody epitope to the transporter, we observed that JHC 1-64 had no detectable effect on NET surface levels. An antibody feeding assay results also showed that TacNET was internalized constitutively to the same Rab11-positive pathway as JHC 1-64-bound NET.

Labeling of live SCG neurons with JHC 1-64 revealed a uniform distribution of NET in the plasma membranes of the extensions and boutons. We also observed a clear labeling of the plasma membrane of the somata, which, to our knowledge, has not been described before. The role of NET in the somata remains to be determined; however, it is attractive to consider that the wide and uniform distribution of NET in SCG neurons reflects the importance of volume transmission for norepinephrine action (58). We should note that a similar uniform distribution in the plasma membrane of SCG neurons and other neuronal preparation was not observed in previous studies based on immunostaining with NET antibodies. Rather, these studies revealed more punctate expression (30, 40, 41, 59).

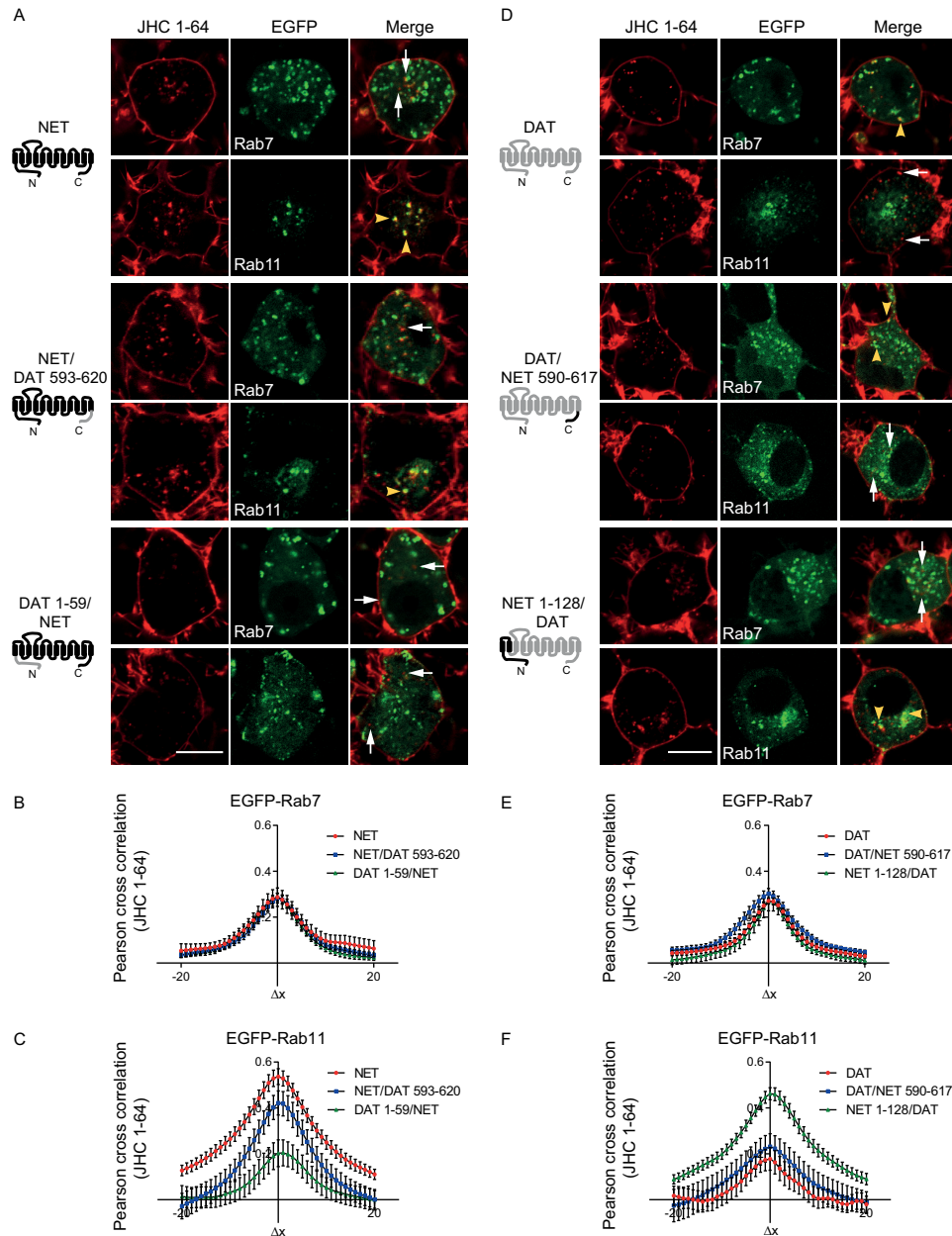


**FIGURE 9. Postendocytic sorting of NET, DAT, and DAT/NET chimeras.** CAD cells expressing wild-type NET, DAT, NET/DAT(593–620), DAT(1–59)/NET, DAT/NET(590–617), or NET(1–128)/DAT together with EGFP-Rab7 or EGFP-Rab11 were incubated with JHC 1-64 (50 nM), followed by internalized at 37 °C for 1 h. *A*, representative confocal live images of the internalized JHC 1-64-labeled NET, NET/DAT(593–620), or DAT(1–59)/NET together with EGFP-Rab7 or EGFP-Rab11. *B* and *C*, quantification of colocalization for the different constructs with EGFP-Rab7 and EGFP-Rab11, respectively, using van Steensel's cross-correlation function. Results are for 20–35 cells for each endosomal marker from 3–5 independent experiments. Introducing the DAT N terminus into NET (DAT(1–59)/NET) decreased colocalization of the transporter with EGFP-Rab11. *Yellow arrowheads*, examples of colocalized vesicles. *White arrowheads*, examples of non-colocalized vesicles. *Scale bar*, 10  $\mu$ m. *D*, representative confocal live images of the internalized JHC 1-64-labeled DAT, DAT/NET(590–617), or NET(1–128)/DAT together with EGFP-Rab7 or EGFP-Rab11. *E* and *F*, quantification of colocalization for the different constructs with EGFP-Rab7 and EGFP-Rab11, respectively, using van Steensel's cross-correlation function. Results are for 20–35 cells for each endosomal marker from 3–5 independent experiments. Introducing the NET N terminus into DAT (NET(1–128)/DAT) increased colocalization of the transporter with EGFP-Rab11. *Yellow arrowheads*, examples of colocalized vesicles. *White arrowheads*, examples of non-colocalized vesicles. *Scale bar*, 10  $\mu$ m. *Error bars*, S.E.

Most likely, this punctate distribution is an artifact of the fixation and permeabilization procedure used for the immunostainings. Our immunostainings also revealed more punctate NET distribution compared with JHC 1-64 labeling of live cells, and fixation and permeabilization also caused the JHC 1-64 labeling to become more punctate (Fig. 1*B*). Of interest, both previous immunostainings and our own showed extensive intracellular NET immunosignals in the somata and in the bou-

tons (16, 30, 40, 41). The presence of such large intracellular pools of NET indirectly suggests that the transporter is dynamically shuffled between intracellular compartments and the plasma membrane. Indeed, we obtained support for such extensive trafficking of NET by demonstrating fast constitutive internalization of NET not only in the cytoplasm of the somata and proximal extensions but also in the cytoplasm of single boutons that conceivably represent presynaptic release and



## Internalization and Recycling of NET

reuptake sites (40, 60, 61). The internalization was moreover increased in SCG neurons upon stimulation with PMA, demonstrating that NET expressed in neurons can be subject to regulation by protein kinase C and other kinases activated by phorbol esters. It was shown before that NET natively expressed in rodent trophoblasts undergoes endocytosis in response to PMA (14), and earlier studies have supported PMA-induced internalization of NET in transfected cells (11, 13, 14, 42). However, PMA-induced trafficking of endogenous NET in neurons has not been demonstrated before.

Upon sequestration from the plasma membrane of SCG neuronal somata, proximal extensions, and boutons, NET showed considerable colocalization with EGFP-tagged Rab11. Rab11 mediates cargo recycling back to the plasma membrane from the pericentriolar recycling endosomes and marks the long loop recycling pathway (52, 54). Altogether, our results suggest that constitutively internalized NET is mainly sorted to the long loop Rab11-dependent recycling pathway and only to a limited extent to degradation. Moreover, we found that the integrity of the Rab11-dependent pathway was important for NET function, because overexpression of a dominant negative mutant (Rab11 S25N) (54, 62) significantly reduced uptake capacity in the SCG neurons. Additional support for sorting of NET to recycling was obtained by expressing NET in CAD cells where confocal imaging and biotinylation experiments showed evidence for the same sorting pattern as in the SCG neurons. Of further interest, Matthies *et al.* (16) showed by use of a NET endodomain antibody that upon amphetamine-induced internalization, NET displays colocalization with both Rab4 and Rab11 in SCG neurons, indicating that amphetamine might increase NET internalization and sorting to both fast and slow recycling pathways (16). Indeed, we also observed some colocalization of internalized JHC 1-64-labeled NET with Rab4 in the boutons of the SGN neurons, indicating that NET also to some degree might recycle via the Rab4 pathway.

We and others have shown that the closely related SLC6 transporters DAT and SERT, like NET, undergo considerable constitutive internalization (18, 20, 22, 23), although a recent study has indicated that DAT only might undergo modest endocytic trafficking *in vivo* (63). Nonetheless, according to our previous findings and in contrast to NET, DAT and SERT are mainly sorted to late endosomes and lysosomes, and, if recycled, they are more likely to follow the Rab4 short loop recycling pathway (22, 24). In contrast, the neuronal glycine transporter (GlyT2) was shown to colocalize with Rab11 and to be efficiently recycled (19). The postendocytic fate of DAT, however, has been debated (18, 23, 24), but our direct comparison of NET and DAT in CAD cells revealed clear differences between the two proteins. In contrast to NET, JHC 1-64-labeled, internalized DAT colocalized mostly with EGFP-Rab7 but somewhat less with EGFP-Rab11 and showed a markedly lower degree of internalization. Importantly, this difference in internalization kinetics is not likely to explain the differential colocalization pattern observed by confocal imaging. Reversible biotinylation experiments indicated that NET is indeed more likely to recycle to a larger degree than DAT and that DAT function, in contrast

to NET function, seems to be unaffected by dominant negative Rab11 mutants (24, 64).<sup>3</sup>

To identify structural elements governing postendocytic sorting and/or internalization rates, we undertook a chimeric approach as previously done to identify domains critical for substrate selectivity and ion dependence in NET and DAT (26, 65). The results suggest that the N termini of NET play critical roles in determining the rate and postendocytic fate of the transporter. Only little is known about intrinsic sorting signals in DAT and NET as well as in other SLC6 family transporters. NET was found to sort to the basolateral membrane, and DAT was found to sort to the apical plasma membrane in polarized epithelial cells. In addition, it was observed that this differential sorting pattern was determined by the N termini (66). An apical localization signal for GAT1 (GABA transporter 1) also appeared to reside in the N terminus, although a basolateral localization signal for GAT2 was located to the C terminus (67–69). The involvement of the N termini in differential targeting in epithelial cells is interesting, but to what degree it directly relates to our observations remains to be investigated. Our insight into structural elements driving constitutive and regulated internalization of SLC6 family transporters is also limited. A short sequence in the DAT C terminus (FREKLAYAIA) was shown to be important for constitutive and PKC-mediated internalization of DAT, but the motif is only partially conserved in NET (70). Interestingly, a short N-terminal segment, which is proximal to TM1 and involved in regulation of transporter conformation (71), was demonstrated to affect constitutive DAT internalization (72), but because the segment is conserved between NET and DAT, it cannot determine the differences between the two transporters observed in this study. It is also unlikely that differences in N-terminal ubiquitination would determine the difference between DAT and NET. N-terminal ubiquitination can regulate PMA-induced DAT internalization (73) but appeared not to affect constitutive internalization and sorting (24).

Striking differences in trafficking itineraries have been observed for other homologous membrane proteins. The G protein-coupled  $\delta$ - and  $\mu$ -opioid receptors are differentially sorted between degradative and recycling pathways following agonist-induced endocytosis (74, 75). In a similar way, dopamine D2 receptors are sorted to degradation, whereas D1 receptors are recycled after agonist-induced endocytosis (76, 77). Notably, sorting of D2 receptors to degradation is not determined by the absence of a recycling signal but by binding of the receptor to GASP (G protein-coupled receptor-associated sorting protein). It would be interesting to see whether similar protein-protein interactions control DAT/NET internalization and sorting. It will also be interesting to clarify the precise biological significance of the distinct trafficking itineraries for NET and DAT, and whether or not these can be related to neuropsychiatric disease or chronic drug use. For example, differential up- and down-regulation of brain NET and DAT, respectively, was reported upon chronic cocaine or methamphetamine exposure in humans (47, 78). For homologous

<sup>3</sup> J. Eriksen and U. Gether, unpublished observation.

receptors, distinct sorting mechanisms are believed to enable differential physiological adaptation to agonist exposure (48, 74, 75). For homologous transport proteins like NET and DAT, it is tempting to suggest that the rapid cycling of NET enables faster adjustment of transporter availability to the immediate cellular needs. It is possible that such tighter control may be required in, for example, peripheral noradrenergic neurons to ensure proper physiological responsiveness of the sympathetic nervous system.

**Author Contributions**—A. V., T. N. J., and U. G. designed the study. A. V., T. N. J., A. H. N., K. L. M., and U. G. were responsible for methodology, and A. V. was responsible for investigation. A. V., M. S., and U. G. wrote the paper.

**Acknowledgments**—We thank Anette Dencker for excellent technical assistance and Dr. Mu-Fa Zou for synthesizing JHC 1-64.

## References

- Iversen, L. L. (1971) Role of transmitter uptake mechanisms in synaptic neurotransmission. *Br. J. Pharmacol.* **41**, 571–591
- Axelrod, J., and Kopin, I. J. (1969) The uptake, storage, release and metabolism of noradrenaline in sympathetic nerves. *Prog. Brain Res.* **31**, 21–32
- Pacholczyk, T., Blakely, R. D., and Amara, S. G. (1991) Expression cloning of a cocaine- and antidepressant-sensitive human norepinephrine transporter. *Nature* **350**, 350–354
- Kristensen, A. S., Andersen, J., Jørgensen, T. N., Sørensen, L., Eriksen, J., Loland, C. J., Strømgaard, K., and Gether, U. (2011) SLC6 neurotransmitter transporters: structure, function, and regulation. *Pharmacol. Rev.* **63**, 585–640
- Chen, N. H., Reith, M. E., and Quick, M. W. (2004) Synaptic uptake and beyond: the sodium- and chloride-dependent neurotransmitter transporter family SLC6. *Pflugers Arch.* **447**, 519–531
- Brøer, S., and Gether, U. (2012) The solute carrier 6 family of transporters. *Br. J. Pharmacol.* **167**, 256–278
- Rumantir, M. S., Kaye, D. M., Jennings, G. L., Vaz, M., Hastings, J. A., and Esler, M. D. (2000) Phenotypic evidence of faulty neuronal norepinephrine reuptake in essential hypertension. *Hypertension* **36**, 824–829
- Shannon, J. R., Flattem, N. L., Jordan, J., Jacob, G., Black, B. K., Biaggioni, I., Blakely, R. D., and Robertson, D. (2000) Orthostatic intolerance and tachycardia associated with norepinephrine-transporter deficiency. *N. Engl. J. Med.* **342**, 541–549
- Hahn, M. K., Robertson, D., and Blakely, R. D. (2003) A mutation in the human norepinephrine transporter gene (SLC6A2) associated with orthostatic intolerance disrupts surface expression of mutant and wild-type transporters. *J. Neurosci.* **23**, 4470–4478
- Kim, C.-H., Hahn, M. K., Joung, Y., Anderson, S. L., Steele, A. H., Mazei-Robinson, M. S., Gizer, I., Teicher, M. H., Cohen, B. M., Robertson, D., Waldman, I. D., Blakely, R. D., and Kim, K.-S. (2006) A polymorphism in the norepinephrine transporter gene alters promoter activity and is associated with attention-deficit hyperactivity disorder. *Proc. Natl. Acad. Sci. U.S.A.* **103**, 19164–19169
- Apparsundaram, S., Galli, A., DeFelice, L. J., Hartzell, H. C., and Blakely, R. D. (1998) Acute regulation of norepinephrine transport: I. Protein kinase C-linked muscarinic receptors influence transport capacity and transporter density in SK-N-SH cells. *J. Pharmacol. Exp. Ther.* **287**, 733–743
- Arapulisamy, O., Mannangatti, P., and Jayanthi, L. D. (2013) Regulated norepinephrine transporter interaction with the neurokinin-1 receptor establishes transporter subcellular localization. *J. Biol. Chem.* **288**, 28599–28610
- Apparsundaram, S., Schroeter, S., Giovanetti, E., and Blakely, R. D. (1998) Acute regulation of norepinephrine transport: II. PKC-modulated surface expression of human norepinephrine transporter proteins. *J. Pharmacol. Exp. Ther.* **287**, 744–751
- Jayanthi, L. D., Samuvel, D. J., and Ramamoorthy, S. (2004) Regulated internalization and phosphorylation of the native norepinephrine transporter in response to phorbol esters: evidence for localization in lipid rafts and lipid raft-mediated internalization. *J. Biol. Chem.* **279**, 19315–19326
- Dipace, C., Sung, U., Binda, F., Blakely, R. D., and Galli, A. (2007) Amphetamine induces a calcium/calmodulin-dependent protein kinase II-dependent reduction in norepinephrine transporter surface expression linked to changes in syntaxin 1A/transporter complexes. *Mol. Pharmacol.* **71**, 230–239
- Matthies, H. J., Moore, J. L., Saunders, C., Matthies, D. S., Lapierre, L. A., Goldenring, J. R., Blakely, R. D., and Galli, A. (2010) Rab11 supports amphetamine-stimulated norepinephrine transporter trafficking. *J. Neurosci.* **30**, 7863–7877
- Mannangatti, P., Arapulisamy, O., Shippenberg, T. S., Ramamoorthy, S., and Jayanthi, L. D. (2011) Cocaine up-regulation of the norepinephrine transporter requires threonine 30 phosphorylation by p38 mitogen-activated protein kinase. *J. Biol. Chem.* **286**, 20239–20250
- Loder, M. K., and Melikian, H. E. (2003) The dopamine transporter constitutively internalizes and recycles in a protein kinase C-regulated manner in stably transfected PC12 cell lines. *J. Biol. Chem.* **278**, 22168–22174
- Fornés, A., Núñez, E., Alonso-Torres, P., Aragón, C., and López-Corcuera, B. (2008) Trafficking properties and activity regulation of the neuronal glycine transporter GLYT2 by protein kinase C. *Biochem. J.* **412**, 495–506
- Eriksen, J., Rasmussen, S. G., Rasmussen, T. N., Vaegter, C. B., Cha, J. H., Zou, M. F., Newman, A. H., and Gether, U. (2009) Visualization of dopamine transporter trafficking in live neurons by use of fluorescent cocaine analogs. *J. Neurosci.* **29**, 6794–6808
- Eriksen, J., Jørgensen, T. N., and Gether, U. (2010) Regulation of dopamine transporter function by protein-protein interactions: new discoveries and methodological challenges. *J. Neurochem.* **113**, 27–41
- Rahbek-Clemmensen, T., Bay, T., Eriksen, J., Gether, U., and Jørgensen, T. N. (2014) The serotonin transporter undergoes constitutive internalization and is primarily sorted to late endosomes and lysosomal degradation. *J. Biol. Chem.* **289**, 23004–23019
- Sorkina, T., Hoover, B. R., Zahner, N. R., and Sorkin, A. (2005) Constitutive and protein kinase C-induced internalization of the dopamine transporter is mediated by a clathrin-dependent mechanism. *Traffic* **6**, 157–170
- Eriksen, J., Bjørn-Yoshimoto, W. E., Jørgensen, T. N., Newman, A. H., and Gether, U. (2010) Postendocytic sorting of constitutively internalized dopamine transporter in cell lines and dopaminergic neurons. *J. Biol. Chem.* **285**, 27289–27301
- Daniels, G. M., and Amara, S. G. (1999) Regulated trafficking of the human dopamine transporter: clathrin-mediated internalization and lysosomal degradation in response to phorbol esters. *J. Biol. Chem.* **274**, 35794–35801
- Giros, B., Wang, Y. M., Suter, S., McLeskey, S. B., Pifl, C., and Caron, M. G. (1994) Delineation of discrete domains for substrate, cocaine, and tricyclic antidepressant interactions using chimeric dopamine-norepinephrine transporters. *J. Biol. Chem.* **269**, 15985–15988
- Lavezzi, G., McCallum, J., Dewey, C. M., and Roche, K. W. (2004) Subunit-specific regulation of NMDA receptor endocytosis. *J. Neurosci.* **24**, 6383–6391
- Brown, T. C., Correia, S. S., Petrok, C. N., and Esteban, J. A. (2007) Functional compartmentalization of endosomal trafficking for the synaptic delivery of AMPA receptors during long-term potentiation. *J. Neurosci.* **27**, 13311–13315
- Biber, K., Klotz, K. N., Berger, M., Gebicke-Härter, P. J., and van Calker, D. (1997) Adenosine A1 receptor-mediated activation of phospholipase C in cultured astrocytes depends on the level of receptor expression. *J. Neurosci.* **17**, 4956–4964
- Savchenko, V., Sung, U., and Blakely, R. D. (2003) Cell surface trafficking of the antidepressant-sensitive norepinephrine transporter revealed with an ectodomain antibody. *Mol. Cell Neurosci.* **24**, 1131–1150
- Naldini, L., Blömer, U., Gage, F. H., Trono, D., and Verma, I. M. (1996) Efficient transfer, integration, and sustained long-term expression of the transgene in adult rat brains injected with a lentiviral vector. *Proc. Natl. Acad. Sci. U.S.A.* **93**, 11325–11329



- Acad. Sci. U.S.A.* **93**, 11382–11388
32. Yamamoto, B. K., and Novotney, S. (1998) Regulation of extracellular dopamine by the norepinephrine transporter. *J. Neurochem.* **71**, 274–280
  33. Morón, J. A., Brockington, A., Wise, R. A., Rocha, B. A., and Hope, B. T. (2002) Dopamine uptake through the norepinephrine transporter in brain regions with low levels of the dopamine transporter: evidence from knock-out mouse lines. *J. Neurosci.* **22**, 389–395
  34. Raiteri, M., Del Carmine, R., Bertolini, A., and Levi, G. (1977) Effect of sympathomimetic amines on the synaptosomal transport of noradrenaline, dopamine and 5-hydroxytryptamine. *Eur. J. Pharmacol.* **41**, 133–143
  35. Cha, J. H., Zou, M. F., Adkins, E. M., Rasmussen, S. G., Loland, C. J., Schoenenberger, B., Gether, U., and Newman, A. H. (2005) Rhodamine-labeled 2 $\beta$ -carbomethoxy-3 $\beta$ -(3,4-dichlorophenyl)tropane analogues as high-affinity fluorescent probes for the dopamine transporter. *J. Med. Chem.* **48**, 7513–7516
  36. Bolte, S., and Cordelières, F. P. (2006) A guided tour into subcellular colocalization analysis in light microscopy. *J. Microsc.* **224**, 213–232
  37. Rajamanickam, J., Annamalai, B., Rahbek-Clemmensen, T., Sundaramurthy, S., Gether, U., Jayanthi, L. D., and Ramamoorthy, S. (2015) Akt-mediated regulation of antidepressant-sensitive serotonin transporter function, cell-surface expression and phosphorylation. *Biochem. J.* **468**, 177–190
  38. Holst, B., Madsen, K. L., Jansen, A. M., Jin, C., Rickhag, M., Lund, V. K., Jensen, M., Bhatia, V., Sørensen, G., Madsen, A. N., Xue, Z., Møller, S. K., Woldbye, D., Qvortrup, K., Haganir, R., Stamou, D., Kjærulf, O., and Gether, U. (2013) PICK1 deficiency impairs secretory vesicle biogenesis and leads to growth retardation and decreased glucose tolerance. *PLoS Biol.* **11**, e1001542
  39. Schramm, N. L., and Limbird, L. E. (1999) Stimulation of mitogen-activated protein kinase by G protein-coupled  $\alpha_2$ -adrenergic receptors does not require agonist-elicited endocytosis. *J. Biol. Chem.* **274**, 24935–24940
  40. Matthies, H. J., Han, Q., Shields, A., Wright, J., Moore, J. L., Winder, D. G., Galli, A., and Blakely, R. D. (2009) Subcellular localization of the antidepressant-sensitive norepinephrine transporter. *BMC Neurosci.* **10**, 65
  41. Sung, U., Apparsundaram, S., Galli, A., Kahlig, K. M., Savchenko, V., Schroeter, S., Quick, M. W., and Blakely, R. D. (2003) A regulated interaction of syntaxin 1A with the antidepressant-sensitive norepinephrine transporter establishes catecholamine clearance capacity. *J. Neurosci.* **23**, 1697–1709
  42. Jayanthi, L. D., Annamalai, B., Samuvel, D. J., Gether, U., Ramamoorthy S. (2006) Phosphorylation of the norepinephrine transporter at threonine 258 and serine 259 is linked to protein kinase C-mediated transporter internalization. *J. Biol. Chem.* **281**, 23326–23340
  43. Maxfield, F. R., and McGraw, T. E. (2004) Endocytic recycling. *Nat. Rev. Mol. Cell Biol.* **5**, 121–132
  44. Schwartz, S. L., Cao, C., Pylpenko, O., Rak, A., and Wandinger-Ness, A. (2007) Rab GTPases at a glance. *J. Cell Sci.* **120**, 3905–3910
  45. Stenmark, H. (2009) Rab GTPases as coordinators of vesicle traffic. *Nat. Rev. Mol. Cell Biol.* **10**, 513–525
  46. Zhang, K., Fishel Ben Kenan, R., Osakada, Y., Xu, W., Sinit, R. S., Chen, L., Zhao, X., Chen, J. Y., Cui, B., and Wu, C. (2013) Defective axonal transport of Rab7 GTPase results in dysregulated trophic signaling. *J. Neurosci.* **33**, 7451–7462
  47. Ding, Y. S., Singhal, T., Planeta-Wilson, B., Gallezot, J. D., Nabulsi, N., Labaree, D., Ropchan, J., Henry, S., Williams, W., Carson, R. E., Neumeister, A., and Malison, R. T. (2010) PET imaging of the effects of age and cocaine on the norepinephrine transporter in the human brain using (S,S)-[<sup>14</sup>C]O-methylreboxetine and HRRT. *Synapse* **64**, 30–38
  48. Gage, R. M., Kim, K. A., Cao, T. T., and von Zastrow, M. (2001) A transplantable sorting signal that is sufficient to mediate rapid recycling of G protein-coupled receptors. *J. Biol. Chem.* **276**, 44712–44720
  49. Rickhag, M., Hansen, F. H., Sørensen, G., Strandfelt, K. N., Andresen, B., Gotfryd, K., Madsen, K. L., Vestergaard-Klewe, I., Ammendrup-Johnsen, I., Eriksen, J., Newman, A. H., Füchtbauer, E. M., Gomeza, J., Woldbye, D. P., Wörtwein, G., and Gether, U. (2013) A C-terminal PDZ domain-binding sequence is required for striatal distribution of the dopamine transporter. *Nat. Commun.* **4**, 1580
  50. González, M. I., Susarla, B. T., Fournier, K. M., Sheldon, A. L., and Robinson, M. B. (2007) Constitutive endocytosis and recycling of the neuronal glutamate transporter, excitatory amino acid carrier 1. *J. Neurochem.* **103**, 1917–1931
  51. Wilcke, M., Johannes, L., Galli, T., Mayau, V., Goud, B., and Salamero, J. (2000) Rab11 regulates the compartmentalization of early endosomes required for efficient transport from early endosomes to the trans-Golgi network. *J. Cell Biol.* **151**, 1207–1220
  52. Chen, W., Feng, Y., Chen, D., and Wandinger-Ness, A. (1998) Rab11 is required for trans-Golgi network-to-plasma membrane transport and a preferential target for GDP dissociation inhibitor. *Mol. Biol. Cell* **9**, 3241–3257
  53. Grant, B. D., and Donaldson, J. G. (2009) Pathways and mechanisms of endocytic recycling. *Nat. Rev. Mol. Cell Biol.* **10**, 597–608
  54. Ullrich, O., Reinsch, S., Urbé, S., Zerial, M., and Parton, R. G. (1996) Rab11 regulates recycling through the pericentriolar recycling endosome. *J. Cell Biol.* **135**, 913–924
  55. Suri, C., Fung, B. P., Tischler, A. S., and Chikaraishi, D. M. (1993) Catecholaminergic cell lines from the brain and adrenal glands of tyrosine hydroxylase-SV40 T antigen transgenic mice. *J. Neurosci.* **13**, 1280–1291
  56. Qi, Y., Wang, J. K., McMillian, M., and Chikaraishi, D. M. (1997) Characterization of a CNS cell line, CAD, in which morphological differentiation is initiated by serum deprivation. *J. Neurosci.* **17**, 1217–1225
  57. Mollenhauer, H. H., Morré, D. J., and Rowe, L. D. (1990) Alteration of intracellular traffic by monensin; mechanism, specificity and relationship to toxicity. *Biochim. Biophys. Acta* **1031**, 225–246
  58. Zoli, M., Jansson, A., Syková, E., Agnati, L. F., and Fuxe, K. (1999) Volume transmission in the CNS and its relevance for neuropsychopharmacology. *Trends Pharmacol. Sci.* **20**, 142–150
  59. Miner, L. H., Schroeter, S., Blakely, R. D., and Sesack, S. R. (2003) Ultrastructural localization of the norepinephrine transporter in superficial and deep layers of the rat prefrontal cortex and its spatial relationship to probable dopamine terminals. *J. Comp. Neurol.* **466**, 478–494
  60. Geffen, L. B., and Livett, B. G. (1971) Synaptic vesicles in sympathetic neurons. *Physiol. Rev.* **51**, 98–157
  61. Livett, B. G. (1973) Histochemical visualization of peripheral and central adrenergic neurones. *Br. Med. Bull.* **29**, 93–99
  62. Stenmark, H., Parton, R. G., Steele-Mortimer, O., Lütcke, A., Gruenberg, J., and Zerial, M. (1994) Inhibition of rab5 GTPase activity stimulates membrane fusion in endocytosis. *EMBO J.* **13**, 1287–1296
  63. Block, E. R., Nuttle, J., Balcita-Pedicino, J. J., Caltagarone, J., Watkins, S. C., Sesack, S. R., and Sorkin, A. (2015) Brain region-specific trafficking of the dopamine transporter. *J. Neurosci.* **35**, 12845–12858
  64. Furman, C. A., Lo, C. B., Stokes, S., Esteban, J. A., and Gnegy, M. E. (2009) Rab 11 regulates constitutive dopamine transporter trafficking and function in N2A neuroblastoma cells. *Neurosci. Lett.* **463**, 78–81
  65. Buck, K. J., and Amara, S. G. (1994) Chimeric dopamine-norepinephrine transporters delineate structural domains influencing selectivity for catecholamines and 1-methyl-4-phenylpyridinium. *Proc. Natl. Acad. Sci. U.S.A.* **91**, 12584–12588
  66. Gu, H. H., Wu, X., Giros, B., Caron, M. G., Caplan, M. J., and Rudnick, G. (2001) The NH<sub>2</sub>-terminus of norepinephrine transporter contains a basolateral localization signal for epithelial cells. *Mol. Biol. Cell* **12**, 3797–3807
  67. Perego, C., Bulbarelli, A., Longhi, R., Caimi, M., Villa, A., Caplan, M. J., and Pietrini, G. (1997) Sorting of two polytopic proteins, the  $\gamma$ -aminobutyric acid and betaine transporters, in polarized epithelial cells. *J. Biol. Chem.* **272**, 6584–6592
  68. Brown, A., Muth, T., and Caplan, M. (2004) The COOH-terminal tail of the GAT-2 GABA transporter contains a novel motif that plays a role in basolateral targeting. *Am. J. Physiol. Cell Physiol.* **286**, C1071–C1077
  69. Muth, T. R., Ahn, J., and Caplan, M. J. (1998) Identification of sorting determinants in the C-terminal cytoplasmic tails of the  $\gamma$ -aminobutyric acid transporters GAT-2 and GAT-3. *J. Biol. Chem.* **273**, 25616–25627
  70. Holton, K. L., Loder, M. K., and Melikian, H. E. (2005) Nonclassical, distinct endocytic signals dictate constitutive and PKC-regulated neurotransmitter transporter internalization. *Nat. Neurosci.* **8**, 881–888
  71. Kniazeff, J., Shi, L., Loland, C. J., Javitch, J. A., Weinstein, H., and Gether, U. (2008) An intracellular interaction network regulates conformational transitions in the dopamine transporter. *J. Biol. Chem.* **283**, 17691–17701

72. Sorkina, T., Richards, T. L., Rao, A., Zahniser, N. R., and Sorkin, A. (2009) Negative regulation of dopamine transporter endocytosis by membrane-proximal N-terminal residues. *J. Neurosci.* **29**, 1361–1374
73. Vina-Vilaseca, A., and Sorkin, A. (2010) Lysine 63-linked polyubiquitination of the dopamine transporter requires WW3 and WW4 domains of Nedd4-2 and UBE2D ubiquitin-conjugating enzymes. *J. Biol. Chem.* **285**, 7645–7656
74. Tanowitz, M., and von Zastrow, M. (2003) A novel endocytic recycling signal that distinguishes the membrane trafficking of naturally occurring opioid receptors. *J. Biol. Chem.* **278**, 45978–45986
75. Whistler, J. L., Enquist, J., Marley, A., Fong, J., Gladher, F., Tsuruda, P., Murray, S. R., and Von Zastrow, M. (2002) Modulation of postendocytic sorting of G protein-coupled receptors. *Science* **297**, 615–620
76. Bartlett, S. E., Enquist, J., Hopf, F. W., Lee, J. H., Gladher, F., Kharazia, V., Waldhoer, M., Mailliard, W. S., Armstrong, R., Bonci, A., and Whistler, J. L. (2005) Dopamine responsiveness is regulated by targeted sorting of D2 receptors. *Proc. Natl. Acad. Sci. U.S.A.* **102**, 11521–11526
77. Vargas, G. A., and Von Zastrow, M. (2004) Identification of a novel endocytic recycling signal in the D1 dopamine receptor. *J. Biol. Chem.* **279**, 37461–37469
78. McCann, U. D., Wong, D. F., Yokoi, F., Villemagne, V., Dannals, R. F., and Ricaurte, G. A. (1998) Reduced striatal dopamine transporter density in abstinent methamphetamine and methcathinone users: evidence from positron emission tomography studies with [<sup>11</sup>C]WIN-35,428. *J. Neurosci.* **18**, 8417–8422